EUROPEAN ORGANISATION FOR PARTICLE PHYSICS

CERN-PPE/93-146
9 August 1993

Improved Measurements of the Neutral Current from Hadron and Lepton Production at LEP

The OPAL Collaboration

Abstract

We present an update with increased statistics to our published analysis of hadronic and leptonic cross sections and of the leptonic forward-backward asymmetries in e^+e^- collisions. The published results were based on a total of 454 000 hadronic and 58 000 leptonic events. This analysis adds 733 000 hadronic and 88 000 leptonic events recorded at the Z^0 peak in 1992 by the OPAL experiment at LEP. A model independent analysis of Z^0 parameters based on an extension of the improved Born approximation leads to tests of lepton universality and gives an interpretation of the results within the Standard Model framework. We also present a model independent test for new physics.

Submitted to Z. Phys. C

The OPAL Collaboration

R. Akers[16], G. Alexander[23], J. Allison[16], K.J. Anderson[9], S. Arcelli[2], A. Astbury[28], D. Axen[29], G. Azuelos[18,a], J.T.M. Baines[16], A.H. Ball[17], J. Banks[16], R.J. Barlow[16], S. Barnett[16], R. Bartoldus[3], J.R. Batley[5], G. Beaudoin[18], A. Beck[23], G.A. Beck[13], J. Becker[10], C. Beeston[16], T. Behnke[27], K.W. Bell[20], G. Bella[23], P. Bentkowski[18], P. Berlich[10], S. Bethke[11], O. Biebel[3], I.J. Bloodworth[1], P. Bock[11], B. Boden[3], H.M. Bosch[11], M. Boutemeur[18], H. Breuker[8,b], P. Bright-Thomas[25], R.M. Brown[20], A. Buijs[8], H.J. Burckhart[8], C. Burgard[27], P. Capiluppi[2], R.K. Carnegie[6], A.A. Carter[13], J.R. Carter[5], C.Y. Chang[17], D.G. Charlton[8], S.L. Chu[4], P.E.L. Clarke[15], J.C. Clayton[1], I. Cohen[23], J.E. Conboy[15], M. Cooper[22], M. Coupland[14], M. Cuffiani[2], S. Dado[22], G.M. Dallavalle[2], S. De Jong[13], L.A. del Pozo[5], H. Deng[17], A. Dieckmann[11], M. Dittmar[4], M.S. Dixit[7], E. do Couto e Silva[12], J.E. Duboscq[8], E. Duchovni[26], G. Duckeck[11], I.P. Duerdoth[16], D.J.P. Dumas[6], P.A. Elcombe[5], P.G. Estabrooks[6], E. Etzion[23], H.G. Evans[9], F. Fabbri[2], B. Fabbro[21], M. Fierro[2], M. Fincke-Keeler[28], H.M. Fischer[3], D.G. Fong[17], M. Foucher[17], A. Gaidot[21], J.W. Gary[4], J. Gascon[18], N.I. Geddes[20], C. Geich-Gimbel[3], S.W. Gensler[9], F.X. Gentit[21], G. Giacomelli[2], R. Giacomelli[2], V. Gibson[5], W.R. Gibson[13], J.D. Gillies[20], J. Goldberg[22], D.M. Gingrich[30,a], M.J. Goodrick[5], W. Gorn[4], C. Grandi[2], F.C. Grant[5], J. Hagemann[27], G.G. Hanson[12], M. Hansroul[8], C.K. Hargrove[7], P.F. Harrison[13], J. Hart[8], P.M. Hattersley[1], M. Hauschild[8], C.M. Hawkes[8], E. Heflin[4], R.J. Hemingway[6], G. Herten[10], R.D. Heuer[8], J.C. Hill[5], S.J. Hillier[8], T. Hilse[10], D.A. Hinshaw[18], J.D. Hobbs[8], P.R. Hobson[25], D. Hochman[26], R.J. Homer[1], A.K. Honma[28,a], R.E. Hughes-Jones[16], R. Humbert[10], P. Igo-Kemenes[11], H. Ihssen[11], D.C. Imrie[25], A.C. Janissen[6], A. Jawahery[17], P.W. Jeffreys[20], H. Jeremie[18], M. Jimack[1], M. Jones[29], R.W.L. Jones[8], P. Jovanovic[1], C. Jui[4], D. Karlen[6], K. Kawagoe[24], T. Kawamoto[24], R.K. Keeler[28], R.G. Kellogg[17], B.W. Kennedy[15], J. King[13], S. Kluth[5], T. Kobayashi[24], D.S. Koetke[8], T.P. Kokott[3], S. Komamiya[24], J.F. Kral[8], R. Kowalewski[8], J. von Krogh[11], J. Kroll[9], P. Kyberd[13], G.D. Lafferty[16], H. Lafoux[21], R. Lahmann[17], J. Lauber[8], J.G. Layter[4], P. Leblanc[18], A.M. Lee[31], E. Lefebvre[18], M.H. Lehto[15], D. Lellouch[26], C. Leroy[18], J. Letts[4], L. Levinson[26], S.L. Lloyd[13], F.K. Loebinger[16], J.M. Lorah[17], B. Lorazo[18], M.J. Losty[7], X.C. Lou[12], J. Ludwig[10], A. Luig[10], M. Mannelli[8], S. Marcellini[2], C. Markus[3], A.J. Martin[13], J.P. Martin[18], T. Mashimo[24], P. Mättig[3], U. Maur[3], J. McKenna[29], T.J. McMahon[1], J.R. McNutt[25], F. Meijers[8], D. Menszner[11], F.S. Merritt[9], H. Mes[7], A. Michelini[8], R.P. Middleton[20], G. Mikenberg[26], J. Mildenberger[6], D.J. Miller[15], R. Mir[12], W. Mohr[10], C. Moisan[18], A. Montanari[2], T. Mori[24], M. Morii[24], U. Müller[3], B. Nellen[3], H.H. Nguyen[9], S.W. O'Neale[1], F.G. Oakham[7], F. Odorici[2], H.O. Ogren[12], C.J. Oram[28,a], M.J. Oreglia[9], S. Orito[24], J.P. Pansart[21], B. Panzer-Steindel[8], P. Paschievici[26], G.N. Patrick[20], N. Paz-Jaoshvili[23], M.J. Pearce[1], P. Pfister[10], J.E. Pilcher[9], J. Pinfold[30], D. Pitman[28], D.E. Plane[8], P. Poffenberger[28], B. Poli[2], T.W. Pritchard[13], H. Przysiezniak[18], G. Quast[27], M.W. Redmond[8], D.L. Rees[8], G.E. Richards[16], M. Rison[5], S.A. Robins[5], D. Robinson[8], A. Rollnik[3], J.M. Roney[28], E. Ros[8], S. Rossberg[10], A.M. Rossi[2], M. Rosvick[28], P. Routenburg[30], K. Runge[10], O. Runolfsson[8], D.R. Rust[12], M. Sasaki[24], C. Sbarra[2], A.D. Schaile[26], O. Schaile[10], W. Schappert[6], F. Scharf[3], P. Scharff-Hansen[8], P. Schenk[4], B. Schmitt[3], H. von der Schmitt[11], M. Schröder[12], C. Schwick[27], J. Schwiening[3], W.G. Scott[20], M. Settles[12], T.G. Shears[5], B.C. Shen[4], C.H. Shepherd-Themistocleous[7], P. Sherwood[15], G.P. Siroli[2], A. Skillman[16], A. Skuja[17], A.M. Smith[8], T.J. Smith[28], G.A. Snow[17], R. Sobie[28], R.W. Springer[17], M. Sproston[20], A. Stahl[3], C. Stegmann[10], K. Stephens[16], J. Steuerer[28], R. Ströhmer[11], D. Strom[19], H. Takeda[24], T. Takeshita[24,c], S. Tarem[26], M. Tecchio[9], P. Teixeira-Dias[11], N. Tesch[3], M.A. Thomson[15], E. Torrente-Lujan[22], S. Towers[28], G. Transtromer[25], N.J. Tresilian[16], T. Tsukamoto[24], M.F. Turner[8], D. Van den plas[18], R. Van Kooten[27], G.J. VanDalen[4], G. Vasseur[21], A. Wagner[27], D.L. Wagner[9], C. Wahl[10], C.P. Ward[5], D.R. Ward[5], P.M. Watkins[1], A.T. Watson[1], N.K. Watson[8], M. Weber[11], P. Weber[6], P.S. Wells[8], N. Wermes[3], M.A. Whalley[1], B. Wilkens[10], G.W. Wilson[4], J.A. Wilson[1], V-H. Winterer[10], T. Wlodek[26], G. Wolf[26], S. Wotton[11], T.R. Wyatt[16], R. Yaari[26], A. Yeaman[13], G. Yekutieli[26], M. Yurko[18], W. Zeuner[8], G.T. Zorn[17].

[1]School of Physics and Space Research, University of Birmingham, Birmingham, B15 2TT, UK
[2]Dipartimento di Fisica dell' Università di Bologna and INFN, Bologna, 40126, Italy
[3]Physikalisches Institut, Universität Bonn, D-5300 Bonn 1, Germany
[4]Department of Physics, University of California, Riverside, CA 92521 USA
[5]Cavendish Laboratory, Cambridge, CB3 0HE, UK
[6]Carleton University, Dept of Physics, Colonel By Drive, Ottawa, Ontario K1S 5B6, Canada
[7]Centre for Research in Particle Physics, Carleton University, Ottawa, Ontario K1S 5B6, Canada
[8]CERN, European Organisation for Particle Physics, 1211 Geneva 23, Switzerland
[9]Enrico Fermi Institute and Dept of Physics, University of Chicago, Chicago Illinois 60637, USA
[10]Fakultät für Physik, Albert Ludwigs Universität, D-7800 Freiburg, Germany
[11]Physikalisches Institut, Universität Heidelberg, Heidelberg, Germany
[12]Indiana University, Dept of Physics, Swain Hall West 117, Bloomington, Indiana 47405, USA
[13]Queen Mary and Westfield College, University of London, London, E1 4NS, UK
[14]Birkbeck College, London, WC1E 7HV, UK
[15]University College London, London, WC1E 6BT, UK
[16]Department of Physics, Schuster Laboratory, The University, Manchester, M13 9PL, UK
[17]Department of Physics, University of Maryland, College Park, Maryland 20742, USA
[18]Laboratoire de Physique Nucléaire, Université de Montréal, Montréal, Quebec, H3C 3J7, Canada
[19]University of Oregon, Dept of Physics, Eugene, Oregon 97403, USA
[20]Rutherford Appleton Laboratory, Chilton, Didcot, Oxfordshire, OX11 0QX, UK
[21]DAPNIA/SPP, Saclay, F-91191 Gif-sur-Yvette, France
[22]Department of Physics, Technion-Israel Institute of Technology, Haifa 32000, Israel
[23]Department of Physics and Astronomy, Tel Aviv University, Tel Aviv 69978, Israel
[24]International Centre for Elementary Particle Physics and Dept of Physics, University of Tokyo, Tokyo 113, and Kobe University, Kobe 657, Japan
[25]Brunel University, Uxbridge, Middlesex, UB8 3PH UK
[26]Nuclear Physics Department, Weizmann Institute of Science, Rehovot, 76100, Israel
[27]Universität Hamburg/DESY, II Inst für Experimental Physik, Notkestrasse 85, 22607 Hamburg, Germany
[28]University of Victoria, Dept of Physics, P O Box 3055, Victoria BC V8W 3P6, Canada
[29]University of British Columbia, Dept of Physics, Vancouver BC V6T 1Z1, Canada
[30]University of Alberta, Dept of Physics, Edmonton AB T6G 2N5, Canada
[31]Duke University, Dept of Physics, Durham, North Carolina 27708-0305, USA

[a]Also at TRIUMF, Vancouver, Canada V6T 2A3
[b]Now at MPI, München, Germany
[c]Also at Shinshu University, Matsumoto 390, Japan

1 Introduction

We present hadronic and leptonic cross sections and leptonic forward-backward asymmetries measured in e^+e^- collisions at a mean centre-of-mass energy of $\sqrt{s}$=91.299 GeV. The data were recorded during 1992 by the OPAL experiment at LEP. The integrated luminosity of the 1992 dataset is approximately 25 pb^{-1}, which doubles the total available. The 1992 data are combined with our published cross sections and asymmetries [1, 2], from data accumulated up until the end of 1991 at centre-of-mass energies within ± 3 GeV of the Z^0 mass, M_Z. This allows an improved determination of electroweak parameters and a more stringent test of the Standard Model. The larger 1992 data sample has enabled more detailed systematic studies to be made, leading to a reduction of the systematic errors for the luminosity measurement and the lepton analyses presented.

A description of the OPAL detector and Monte Carlo programs is given in section 2. The luminosity measurement and the hadronic and leptonic event selections are described in sections 3, 4 and 5, respectively. The results of the LEP energy calibration are given in section 6 and the determination of electroweak parameters is presented in section 7. Finally, the results are summarized in section 8.

2 The OPAL Detector and Simulation

The OPAL detector is described in detail elsewhere [3]. The trajectories of charged particles are measured using a precision vertex drift chamber, a jet chamber and z-chambers, inside a solenoidal coil. This is surrounded by a time-of-flight counter array and a lead glass electromagnetic calorimeter with a presampler, which measures the positions and energies of showering particles. Outside this are a hadron calorimeter and four layers of muon chambers. Forward detectors are used for measuring the luminosity. A right-handed coordinate system is adopted by OPAL, where the x axis points to the centre of the LEP ring, and positive z is along the electron beam direction. The angles θ and ϕ are the polar and azimuthal angles, respectively.

For the generation of Monte Carlo events for the process $e^+e^- \rightarrow$ hadrons we used the JETSET [4] and HERWIG [5] programs with parameter sets optimized by a study of global event shape variables in OPAL data [6]. The KORALZ [7] program was used for $e^+e^- \rightarrow \mu^+\mu^-$ and $e^+e^- \rightarrow \tau^+\tau^-$, and BABAMC [8] and BHLUMI [9] for the process $e^+e^- \rightarrow e^+e^-$. The detector response was simulated by a program [10] that treated in detail the detector geometry and material as well as the effects of detector resolution and efficiency. The simulated events were then reconstructed by the same procedure that was used to analyse the OPAL data.

3 The Luminosity Measurement

The integrated luminosity was determined from small-angle Bhabha scattering events observed in the forward detectors [11], using essentially the same procedure as for the 1991 data [1]. Each forward detector consists of three major elements: a calorimeter which measures the energy and position of electromagnetic showers; three layers of proportional tube chambers, situated behind the four radiation length presampler section of the calorimeter, which give better spatial resolution and are used to define the acceptance for the Bhabha selection; and two planes of drift chambers in front of the calorimeter which are used to survey the precise positions of the tube chambers.

In [1], the largest contribution to the systematic error (0.30%) resulted from inhomogeneity in the reconstruction of clusters in the proportional tube chambers and evidence for a shift in the survey of one drift chamber quadrant. In order to reduce this uncertainty, the 1992 data have been analysed using new tube chamber reconstruction algorithms, taking advantage of the improved understanding of the detector. As a result the tube chamber inefficiency has decreased from 2.0% to 1.2%, in agreement with Monte Carlo simulation, and the resolution has improved from 3.5 mm to 2.0 mm.

Another effect has been to improve the precision of the drift chamber survey of the locations of the tube chambers. The images of the drift chamber sense wires are located in the tube coordinate system by two methods of analysis, with largely independent systematic errors. In [1] the dominant contribution to the systematic errors on these quantities arose from the differences in the results of the two methods. Using the new reconstruction algorithms the two methods gave consistent results. The mean positions of the two sense wires were determined with precisions of 56 μm and 80 μm, respectively (previously 98 μm and 118 μm), resulting in a reduction of the contribution to the systematic uncertainty in the luminosity from 0.21% to 0.12%. The uncertainty in the absolute positions of the ϕ boundaries of the Bhabha acceptance contributed a further 0.11%, giving a total systematic error on the luminosity due to uncertainties in the locations of the tube chambers of 0.17%.

In our previous analysis the separation of the drift chamber sense wires in diagonally opposite chambers at the same end was measured with a precision of 91 μm. At the end of 1992 an optical survey of the drift chamber support structure was performed by the CERN metrology laboratory, reducing this uncertainty to 42 μm.

As in our previous analyses[1, 2] the effect of inhomogeneity in the tube chamber reconstruction was estimated by dividing the acceptance in ϕ into 8 identical telescopes and determining a luminosity from each. The rms variation of the 8 calculated luminosities was 0.67% (previously 0.90%). Assuming that each telescope gives an independent measurement of the luminosity, the error on the overall luminosity is estimated to be 0.25%. This error includes a contribution of 0.18% from statistics and so the remaining 0.17% is assigned as a systematic error (previously 0.30%). Similar estimates of the systematic error were obtained when the acceptance was divided into 16 and 32 telescopes. Figure 1 shows the fraction of the total number of Bhabha events for each telescope for the case when the acceptance is divided into 8.

Using the new tube reconstruction algorithms the cross section for the Bhabha event selection was determined to be 12.705 $\pm$ 0.014 nb from Monte Carlo. The analysis of six distinct Monte Carlo datasets, generated using different versions of the detector simulation program, GEANT [12], or with minor differences in the assumed detector geometry, gave different values of the cross section (χ^2 of 10.75 for 5 degrees of freedom). Since the number of generated events in individual Monte Carlo datasets was insufficient to allow further investigation, the statistical uncertainties were scaled so that χ^2/d.o.f.= 1. The effect of this additional contribution was to increase the systematic uncertainty on the Monte Carlo cross section from 0.20% (estimated from the variation of the luminosity with cut values) to 0.23%.

The individual contributions to the error on the absolute luminosity are listed in Table 1. These were added in quadrature to give an overall experimental error of 0.41%. Of this, 0.22% was due to the finite data and Monte Carlo statistics. When the theoretical uncertainty of 0.3% is included the final error on the 1992 luminosity becomes 0.51%. The correlation coefficient between the errors on the 1991 [1] and 1992 luminosities is 0.50. In estimating this the systematic errors obtained from the '8 telescope' analysis for the two years were taken to be uncorrelated.

4 The Hadronic Decay Channel

From the 1992 data, 733 059 multihadronic events were selected using the same criteria as described in our previous publication [1]. The correction factors that account for selection efficiency and background are listed in Table 2. The overall correction, f, was 1.0011 with an uncertainty $\Delta f/f = 0.20\%$. The hadronic cross section is given in Table 6.

The background contamination from non-resonant processes was estimated from the data as described in [1]; here the 1991 data were used to evaluate the dependence on centre-of-mass energy. This resulted in a background estimate of 0.060 ± 0.016 nb.

Possible failures in the data acquisition system and in the reconstruction program for high multiplicity events were investigated. An upper limit of 0.04% on the inefficiency due to such failures was obtained and assigned as a systematic error.

The influence of accidental hits in the forward detector calorimeter on the selection were checked by comparing different selection criteria that do not use the forward detector clusters [2]. No systematic effect was found within the 0.05% statistical accuracy, which was assigned as a systematic error.

5 The Leptonic Decay Channels

The analysis of leptonic final states was performed using techniques very similar to those described in our previous publications [1, 2]. Events were required to lie within the angular ranges $|\cos\theta| < 0.70$, $|\cos\theta| < 0.95$ and $|\cos\theta| < 0.90$ for the e^+e^-, $\mu^+\mu^-$ and $\tau^+\tau^-$ channels, respectively. The factors by which the selected numbers of candidate events were corrected in order to account for experimental efficiency and background are given in Tables 3, 4 and 5, for electron, muon and tau pairs, respectively. The leptonic cross sections are given in Table 6. In the case of muon and tau pairs the total production cross section is quoted. Corrections for the selection efficiency and geometrical acceptance for these analyses were evaluated using Monte Carlo events generated with the KORALZ program. In the case of electron pairs the cross section is quoted within the geometrical acceptance and acollinearity cuts, corrected for selection inefficiency and backgrounds.

For the measurement of the forward-backward asymmetry, events were required to have acollinearity angles of less than 10° for the e^+e^- channel and less than 15° for the $\mu^+\mu^-$ and $\tau^+\tau^-$ channels. For the $\mu^+\mu^-$ and $\tau^+\tau^-$ channels the forward-backward asymmetry was calculated using an unbinned maximum likelihood fit to the angular distribution. This was checked by simply counting the numbers of forward and backward events. For the e^+e^- channel, in the absence of a convenient parametrization for the differential cross section, the forward-backward asymmetry was calculated with the simple counting method. The measured leptonic forward-backward asymmetries within the geometrical acceptance are given in Table 7. The numbers of events used in the asymmetry measurements are larger than for the cross sections since less stringent requirements on the status of the detector were needed. This was because a precise knowledge of neither the absolute selection efficiency nor the luminosity was required for the asymmetry analysis.

The increased data sample collected in 1992 allowed the systematic studies described in [1, 2] to be repeated with increased precision. A number of new studies were performed. This, together with continual improvements made in both the performance and understanding of the OPAL detector, is reflected in the reduced systematic errors given in the tables. In the following three sections we describe briefly the most significant improvements for each leptonic channel.

5.1 The e^+e^- Channel

Electron pair events were selected using very similar criteria to those in [1]. Candidate electrons were identified by the signature of a high energy electromagnetic cluster associated with a charged track. Events were required to contain two electron candidates with an acollinearity of less than 10°. Cuts on the number of electromagnetic clusters and the number of charged tracks were used to reject hadronic events. A requirement of high visible energy was used to remove the remaining backgrounds, in particular that from tau pair events. Since our previous publication [1], a modification has been made to the minimum electromagnetic cluster energy cut. In the previous analysis, two electromagnetic clusters were required to satisfy $E > 0.25\sqrt{s}$. In the present analysis, this condition has been changed to $E_1 > 0.20\sqrt{s}$ and $E_2 > 0.10\sqrt{s}$, where E_1 and E_2 refer to the highest and second highest cluster energy respectively. This modification avoids the loss of events ($\sim 0.05\%$) exclusively due to the cluster energy cut. With these selection criteria, a total of 25 280 e^+e^- candidates were selected from the 1992 data sample, within an acceptance of $|\cos\theta| < 0.70$ and acollinearity $< 10°$.

The dominant systematic error quoted in [1] was due to the uncertainty in determining the edge of the acceptance. Based on the larger data sample collected in 1992, we were able to repeat the studies of this problem described in our previous publication with better statistical precision. In addition we examined the θ distributions measured by high quality tracks for the electrons inside and outside the $\cos\theta$ cut defined by the electromagnetic cluster measurement. From these studies, the error of the cross section due to the uncertainty on the edge of the acceptance was reduced to 0.12%.

The e^+e^- events were separated from the $\tau^+\tau^-$ background using a cut on the total electromagnetic energy at $0.80\ \sqrt{s}$, as shown in Figure 2-a. Since there is a small discrepancy between data and Monte Carlo distributions in the region of the cut, the inefficiency was determined by studying the events which failed the energy cut. In Figures 2-b and c, distributions of the acoplanarity and the sum of the charged track momenta are shown for these events. The excesses of data over Monte Carlo simulation are due to e^+e^- events. We estimated an additional inefficiency of 0.30%, above the 0.06% predicted by the simulation, giving a total of $0.36 \pm 0.11\%$.

Similarly the tau pair background was studied using a subsample of the accepted e^+e^- candidates for which the background was enhanced by requiring high acoplanarity and low momenta. An extra 0.10% was estimated, above the 0.28% predicted by Monte Carlo simulation, giving a total tau pair background of $0.38 \pm 0.11\%$.

At least two of the high energy electromagnetic clusters were required to be associated with charged tracks within 5° in ϕ and 10° in θ. Monte Carlo simulation was used to measure the inefficiency for finding matched charged tracks and the causes of the missing tracks in $e^+e^- \to e^+e^-$ events were also studied in detail. It was found that the Monte Carlo simulated well both the fraction of very low energy electrons in the $e^+e^-\gamma$ final state, and the fraction of electrons which lose energy due to hard bremsstrahlung in the material before the central tracking chambers. A discrepancy was observed between data and Monte Carlo for the events which, in spite of the existence of two or more charged tracks, contained less than two electromagnetic clusters matched to tracks. From these studies, we obtained an additional tracking inefficiency of 0.15% to be added to the Monte Carlo estimate of 0.34%, making a total correction of $0.49 \pm 0.09\%$.

A search for e^+e^- events rejected due to the low multiplicity requirement was performed in the region just above the multiplicity cut, by selecting events with either high electromagnetic energy or high track momenta. A small inefficiency of $0.01 \pm 0.01\%$ was found.

The full set of correction factors, valid within the angular acceptance of $|\cos\theta| < 0.70$ and

acollinearity $< 10^\circ$, together with the corresponding systematic uncertainties are summarized in Table 3. The overall correction, f, was 1.0045 with an uncertainty $\Delta f/f = 0.22\%$.

The sign of the charge of the particles was determined from tracks in the central detector. A small fraction ($\sim 1.5\%$) had the same sign assigned for both tracks. As in [1], an alternative method of charge determination was applied to these events, which used the acoplanarity between the two electromagnetic clusters. The efficiency for correct charge assignment using the acoplanarity was estimated from the data and using Monte Carlo simulation. The uncertainty from this was found to be negligible. Other sources of possible bias on the forward-backward asymmetry were studied using similar methods to those used for the geometrical acceptance, described above. As a result of all these studies we assigned an uncertainty of 0.002 to the asymmetry measurement.

For the analyses in section 7, the program ALIBABA [13] is used to predict the t-channel and s-t interference contributions to the $e^+e^- \to e^+e^-$ cross section. In order to check this program we have extended our e^+e^- selection, using slightly modified cuts, out to $|\cos\theta| < 0.90$, where QED t-channel contributions dominate. Figure 3 shows the angular distribution of the data after correction for inefficiency and backgrounds. It agrees well with the ALIBABA prediction.

5.2 The $\mu^+\mu^-$ Channel

Muon pair events were selected within the range $|\cos\theta| < 0.95$ using selection criteria unchanged since our previous publication [1]. Candidate muon pairs were required to contain at least two tracks having a momentum of greater than 6 GeV, matched to the beam interaction point and identified as muons by at least one outer detector (electromagnetic calorimeter, hadron calorimeter or muon chambers). Multihadrons were rejected by requirements on the charged track multiplicity. Remaining tau pair and two photon backgrounds were rejected by a requirement that the visible energy, defined as the sum of the two highest momentum tracks plus the highest energy electromagnetic cluster, be at least $0.60\ \sqrt{s}$.

These criteria selected 34 259 events from the 1992 data. As a result of larger data and Monte Carlo samples the statistical sensitivity of the systematic studies has been improved leading to reduced uncertainty. Better use of the jet chamber track information on poorly constrained tracks has led to a reduction in the cosmic ray background fraction from $0.20\pm0.05\%$ to $0.03\pm0.02\%$. More accurate modelling of the hadron calorimeter and thus of the pion punchthrough simulation resulted in a decrease of the tau pair background estimate from $1.15\pm0.15\%$ to $0.96\pm0.10\%$. The signal efficiency measured from Monte Carlo has also increased from $91.07\pm0.09\%$ to $91.40\pm0.06\%$, mainly due to improvements in track reconstruction. These are discussed in more detail below.

The two dominant systematic errors reported previously remain the largest, these being the estimation of the tau pair background in the sample and the estimation of the effect of track reconstruction problems in the regions close to the jet chamber sense wire planes.

As in [1], the predicted background from $e^+e^- \to \tau^+\tau^-$ was checked by studying the visible energy, acoplanarity and acollinearity distributions in subsamples of the selected muon pair candidates for which the level of background was enhanced. Figure 4-a shows the visible energy. In the region between 0.60 and 0.80 $\sqrt{s}$ there were 215 events in the data, equivalent to 45% of the expected tau pair background, and 197 events predicted by the Monte Carlo simulation, of which 97% were tau pair events. A further check was performed on the modelling of the tau pair background using an independent sample of purely tau pair events, selected by demanding a final state electron and muon. A comparison between data and Monte Carlo visible energy distributions showed good agreement

above 0.50 $\sqrt{s}$ (Figure 4-b). In the region of visible energy between 0.60 and 0.90 $\sqrt{s}$ there were 271 events in the data and 283 in Monte Carlo, which were all simulated tau pairs. An uncertainty on the predicted tau pair background level of 0.10% was estimated.

The fraction of data events lost from tracking inefficiencies was studied using an alternative muon pair selection which was almost independent of the central tracking, based on highly collinear hits in the outer detectors [1]. Due to improved reconstruction of tracks close to jet chamber sense wire planes this fraction was reduced from 1.05% to 0.75%. However, the improvements were found to affect data and Monte Carlo differently, leading to a greater discrepancy between the observed and predicted fractions. The correction derived from this discrepancy has thus increased from $0.33\pm0.11\%$ to $0.48\pm0.10\%$. The error on this correction arises from the uncertainty in the efficiency of the alternative muon pair selection.

The full set of correction factors for the muon pair cross section measurement, together with the corresponding systematic uncertainties are summarized in Table 4. The overall correction factor, f, was 1.0903 with an uncertainty $\Delta f/f = 0.19\%$.

Additional event selection criteria were applied for the forward-backward asymmetry measurement. To suppress radiative events, the acollinearity had to be less than 15^0, which rejected 1.26% of the $\mu^+\mu^-$ events. To ensure unambiguous charge determination, the events were required to contain exactly two oppositely charged tracks, which rejected a further 1.32% of $\mu^+\mu^-$ events. To ensure a high quality polar angle measurement, tracks in the barrel region used to determine $\cos\theta$ had to have both z-chamber and vertex chamber z information. Failing this, if matched hits were found in the barrel muon chambers then these hits were used in combination with the beam interaction point to determine the polar angle. In 0.21% of the events neither track could be used.

The asymmetry was measured using a maximum likelihood fit to the polar angle distribution, using tracks of randomly chosen charge. The systematic uncertainties of the measurement were studied by comparing the asymmetry determined using only positive tracks to that using only negative tracks in a sample where both tracks had good $\cos\theta$ measurements. No significant difference was found. Additionally, the acoplanarity measured in the muon chambers was used as an alternative method of charge determination, and the quality requirements on the barrel tracks were varied. For each of these samples, the result of the fit was also compared with a simple counting method determination of the asymmetry. As a result of these checks, an uncertainty of 0.001 was assigned to the asymmetry measurement.

5.3 The $\tau^+\tau^-$ Channel

Tau pair events were selected within the angular range $|\cos\theta| < 0.90$ using criteria that have remained unchanged since our previous publications [1, 2]. Events were required to contain two back-to-back, collimated, low multiplicity jets identified using information from the central tracking chambers and the electromagnetic calorimeters. Time-of-flight measurements were used to reject cosmic ray events and muon identification to reject $e^+e^- \to \mu^+\mu^-$. The remaining backgrounds from multihadrons, two-photon processes and $e^+e^- \to e^+e^-(\gamma)$ were rejected using multiplicity cuts, and demanding the two jets to be narrow, with an acollinearity of less than 15^0. These criteria selected 28 553 events from the 1992 data.

The uncertainty in determining the edge of the geometrical acceptance was studied by comparing the number of events accepted when tracks only, clusters only or both tracks and clusters were used to reconstruct the $\tau^+\tau^-$ pair event axis. The Monte Carlo simulation reproduced the data to within

0.10%. Taking into account the 2 mrad angular resolution of the track measurement a systematic error of 0.17% was assigned.

Backgrounds were checked by selecting subsamples of the candidate tau pair events in which the background fraction of a given source was enhanced [2]. The increased data and Monte Carlo statistics enabled us to perform more extensive studies, resulting in reduced systematic errors on the background estimates.

Hadronic events were rejected using multiplicity cuts [2]. To assess the residual hadronic background the distribution of the sum of the invariant masses of the two jets, reconstructed using both tracks and clusters, was investigated in the data for all topologies other than the 1-1 and 1-3 topologies (1 or 3 charged tracks in each jet). In the region of high invariant masses the tau pair contribution was assessed using the Monte Carlo simulation and subtracted. It was also necessary to subtract the contributions from tau pair events containing multiple hard photons or four fermions in the final state, which were not simulated by the Monte Carlo program. Their magnitude was estimated from the mass distribution of the data with 1-3 topology. The hadronic background was estimated to be $0.51 \pm 0.14\%$. This estimate was nearly free from uncertainties arising from Monte Carlo modelling of fragmentation.

The overlaps between the $\tau^+\tau^-$ selection and the e^+e^- and $\mu^+\mu^-$ selections were examined using a data sample which contained e^+e^-, $\mu^+\mu^-$ and $\tau^+\tau^-$ events within the same geometrical acceptance. Similar studies to those described in subsections 5.1 and 5.2 were performed. The background from muon pair events misidentified as tau pairs due to track reconstruction problems resulted in a correction of 0.16% to the Monte Carlo prediction and a total $\mu^+\mu^-$ background of $0.98 \pm 0.11\%$. The small loss of tau pair events due to misclassification as muon pairs was found to be correctly simulated by the Monte Carlo to within 0.08%. The residual e^+e^- background was investigated using a similar technique to that described in subsection 5.1. Near the edge of calorimeter modules, an excess of data over Monte Carlo prediction of $0.27 \pm 0.08\%$ was observed, giving a total background of $0.41 \pm 0.15\%$.

To evaluate the loss of tau pair events due to the cut on the total shower energy of $0.80\sqrt{s}$ this distribution was studied in detail (Figure 5-a). The high shower energy region was populated by e^+e^- background and also by $\tau \to \rho\nu$ decays, where the π^0 from the subsequent $\rho \to \pi\pi$ decay carried most of the energy, resulting in a low momentum charged pion in such events. Further cuts were applied to suppress the e^+e^- background. Figures 5-b and c show the distribution after requiring that either of the tau jets have track momentum less than 0.40 of the beam energy and, in addition, that the acoplanarity angle be greater than 0.5^0. A small discrepancy between data and the simulated distributions beyond the cut point resulted in a correction of $0.12 \pm 0.06\%$ to the inefficiency evaluated by Monte Carlo.

The dominant non-resonant background processes were $e^+e^- \to e^+e^-e^+e^-$ and $e^+e^- \to e^+e^-\mu^+\mu^-$. These were studied using Monte Carlo simulation and from a subsample of the tau pair candidates containing a pair of final state electrons or muons. By comparing the distributions of the missing momentum vector the Monte Carlo prediction was found to be good to within 0.05%.

The full set of correction factors and the corresponding systematic uncertainties are summarized in Table 5. The overall correction, f, was 1.3024 with an uncertainty $\Delta f/f = 0.44\%$. The anticorrelation of uncertainties due to cross-over of events from one leptonic channel into another was 0.14% between the $\mu^+\mu^-$ and $\tau^+\tau^-$ samples and 0.09% between the e^+e^- and $\tau^+\tau^-$ channels.

For the forward-backward asymmetry measurement, events in which the two taus were assigned the same charge sign were not used and at least one tau was required to have a charge of ± 1. This rejected 1.9% of the $\tau^+\tau^-$ events. The resulting asymmetry measurement was corrected by -0.001 ± 0.001 to

account for the asymmetry of the e^+e^- background. Possible biases to the asymmetry measurement were examined by comparing the results when tracks only, clusters only or both tracks and clusters were used to reconstruct the direction of the $\tau^+\tau^-$ pair, and also from comparison of results obtained using the polar angle of the τ^+, the τ^- or the average of the two. An uncertainty of 0.002 was estimated for the tau pair asymmetry measurement.

6 LEP Energy Calibration

A precise calibration of the LEP energy scale was achieved in 1991 resulting in a systematic uncertainty of 6 MeV on M_Z [14]. The calibration of the LEP energy scale in 1992 [15] was performed using a similar procedure. In 1992, however, calibrations with resonant depolarization were successful only late in the year and showed a large spread resulting in an error of ± 18 MeV on the centre-of-mass energy. This causes an uncertainty of ± 0.02 nb on the hadronic pole cross section and an uncertainty of ± 0.001 on the forward-backward asymmetry at the Z^0 pole of $e^+e^- \to \mu^+\mu^-$ and $e^+e^- \to \tau^+\tau^-$, which is fully anti-correlated with the uncertainty of ∓ 0.001 on the forward-backward asymmetry of $e^+e^- \to e^+e^-$.

The spread of the centre-of-mass energies, due to the energy spread of the particles in the beams, was 46 ± 5 MeV for the running periods in 1990-91 and 51 ± 5 MeV for the running period in 1992 [15]. Our quoted cross sections and asymmetries are not corrected for the energy spread. It was taken into account by correcting the measured cross sections in the fitting procedure as described in our previous publication [1].

7 Determination of Electroweak Parameters

Electroweak parameters were determined from the 1992 measurements described in the previous sections combined with our 1991 results (Tables 6-10 in [1]), our 1990 hadronic and leptonic cross sections (Tables 7-10 in [2]) and our combined 1989/1990 leptonic asymmetries (Tables 11-13 in [2]). The procedure used to fit the cross sections and the leptonic asymmetries was essentially the same as that described in our previous publications [1, 2]. The systematic errors of our measurements reported previously were in general larger than those of the 1992 data. The 1992 systematic errors for the hadronic and leptonic event selections were treated as common uncertainties among the data sets for 1992, 1991 and 1990. The correlation of the systematic errors for the luminosity measurement in 1992 and 1991 is given in section 3. As described in our previous publication [1] we did not include the information from the absolute luminosity measurement in 1990 and we also did not use the 1990 absolute energy calibration.

The theoretical parametrizations of the total and differential cross sections for the processes $e^+e^- \to$ hadrons, $e^+e^- \to \mu^+\mu^-$, $e^+e^- \to \tau^+\tau^-$ and the contribution of s-channel diagrams to $e^+e^- \to e^+e^-$ were obtained using the program ZFITTER [16]. For the process $e^+e^- \to e^+e^-$ we used the program ALIBABA [13] to describe the contributions from the t-channel diagrams and from s-t interference. These were then added to the s-channel differential cross sections calculated by ZFITTER. Following the recommendation in [13], an uncertainty of 0.5% was assigned to these contributions.

The analysis methods presented in subsections 7.1–7.3 remained unchanged since our last publication [1], to which the reader is referred for formulae, details of the fits and parameter definitions. Our earlier data included some off-peak luminosity, recorded at centre-of-mass energies within ± 3 GeV

of $M_{\rm Z}$. Since all the 1992 data were accumulated close to the $\rm Z^0$ peak, the precision of those electroweak parameters which are determined by off-peak data ($M_{\rm Z}$, $\Gamma_{\rm Z}$, $C^a_{\gamma{\rm Z}}$ and $C^s_{\gamma{\rm Z}}$) remains unchanged compared to [1].

7.1 Extended Improved Born Approach

Table 8 (c.f. Table 11 in [1]) gives the results of fits to the combined data set of hadronic and leptonic cross sections and leptonic forward-backward asymmetries. Parameter correlation matrices are given in the Appendix. The values in the second column of Table 8 were obtained from a 15 parameter fit with $M_{\rm Z}$, $\Gamma_{\rm Z}$, $\sigma^{\rm pole}_{\rm had}$, and the 12 C parameters [1] ($C^s_{\gamma{\rm Z}}$, $C^a_{\gamma{\rm Z}}$, $C^a_{\rm ZZ}$ and $C^s_{\rm ZZ}$ individually for each leptonic species) as free parameters. The values obtained from the different leptonic species for corresponding parameters are consistent with one another, supporting the hypothesis of lepton universality. The most precise test of lepton universality is obtained from the ratio of $C^s_{\rm ZZ}$ parameters for different leptonic species, as the overall normalization error cancels. In the improved Born approximation the ratio of $C^s_{\rm ZZ}$ parameters can be expressed as:

$$R_{\ell/\tau} = \frac{C^s_{\rm ZZ}(\ell^+\ell^-)}{C^s_{\rm ZZ}(\tau^+\tau^-)} \equiv \frac{\hat{g}_a^{\ell\,2} + \hat{g}_v^{\ell\,2}}{\hat{g}_a^{\tau\,2} + \hat{g}_v^{\tau\,2}} \qquad \text{for } \ \ell = \text{e or } \mu\,.$$

The result of our measurement is:

$$\begin{aligned} R_{e/\tau} &= 1.007 \pm 0.010 \\ R_{\mu/\tau} &= 1.0089 \pm 0.0087\,. \end{aligned}$$

Column three of Table 8 gives the results for a 7 parameter model-independent fit when lepton universality was assumed explicitly by imposing $C(\rm e^+e^-) \equiv C(\mu^+\mu^-) \equiv C(\tau^+\tau^-)$ for each of the four C parameters.

Figure 6 shows a comparison of the results with the Standard Model prediction for the fitted parameters. Good agreement is observed for all parameters. The largest deviation, in $C^a_{\gamma{\rm Z}}$, remains unchanged from [1] since it is determined by off-peak data.

The effective leptonic couplings, $\hat{g}_a^{\ell\,2}$ and $\hat{g}_v^{\ell\,2}$, can be determined from the C parameters, assuming lepton universality and the improved Born approximation [1]. The result is:

$$\hat{g}_v^{\ell\,2} = 0.00118 \pm 0.00026 \qquad\qquad \hat{g}_a^{\ell\,2} = 0.2504 \pm 0.0013\,.$$

7.2 Derived Parameters

The partial decay widths $\Gamma_{\rm had}$, Γ_{ee}, $\Gamma_{\mu\mu}$ and $\Gamma_{\tau\tau}$, as given in Table 9, have been obtained by a parameter transformation from the parameters $C^s_{\rm ZZ}(\rm e^+e^-)$, $C^s_{\rm ZZ}(\mu^+\mu^-)$, $C^s_{\rm ZZ}(\tau^+\tau^-)$, $M_{\rm Z}$, $\Gamma_{\rm Z}$ and $\sigma^{\rm pole}_{\rm had}$ [1] from our model independent fit. The leptonic partial widths are consistent with each other, as already observed in the results for the $C^s_{\rm ZZ}$ parameters.

For the decay width of the $\rm Z^0$ into invisible final states, $\Gamma_{\rm inv}$, we obtain:

$$\Gamma_{\rm inv} = \Gamma_{\rm Z} - \Gamma_{\rm had} - (3+\delta_m)\Gamma_{\ell\ell} = 490.3 \pm 7.3 \text{ MeV}\,,$$

where we define $\Gamma_{\ell\ell}$ as the partial width of the Z^0 for the decay into a pair of massless charged leptons and $\delta_m = -0.0023$ [17] represents a small correction for the mass of the tau lepton. For the ratio $\Gamma_{\rm inv}/\Gamma_{\ell\ell}$ we obtain:

$$\Gamma_{\rm inv}/\Gamma_{\ell\ell} = 5.868 \pm 0.090\,.$$

Combining the measured value of $\Gamma_{\rm inv}/\Gamma_{\ell\ell}$ with the Standard Model prediction for $\Gamma_{\nu\nu}/\Gamma_{\ell\ell}$=1.992$\pm$0.003, where the error refers to a variation of the mass of the top quark $M_{\rm t}$ in the interval $50 < M_{\rm t}\,({\rm GeV}) < 230$ and the mass of the Higgs boson $M_{\rm H}$ in the interval $60 < M_{\rm H}\,({\rm GeV}) < 1000$, we obtain for the number of light neutrino generations:

$$N_\nu = 2.946 \pm 0.045({\rm exp.}) \pm 0.005(M_{\rm t}, M_{\rm H})\,.$$

We also apply a parameter transformation to our model independent fit to describe our data in terms of the standard LEP parameter set, $M_{\rm Z}$, $\Gamma_{\rm Z}$, $\sigma^{\rm pole}_{\rm had}$, R_ℓ and $A^{\rm pole}_{\rm FB}$ [1]. The results are given in Table 10. Parameter correlation matrices are given in the Appendix. Figure 7 shows, for each leptonic species, the resulting one standard deviation contours in the R_ℓ-$A^{\rm pole}_{\rm FB}$ plane. The comparison of the R_ℓ values for the individual leptonic species provides a test of lepton universality with similar sensitivity to the ratio of $C^s_{\rm ZZ}$ parameters, as the overall normalization error cancels in R_ℓ. These results are again compatible with lepton universality.

7.3 Standard Model Fits

In this section we compare the data to the Standard Model prediction and infer constraints on the model's unknown input parameters. From the fit [1] to our data we obtain:

$$\begin{aligned} M_{\rm t} &= 132^{+41\,+24}_{-48\,-18}\ {\rm GeV} \\ \alpha_s(M_{\rm Z}^2) &= 0.124 \pm 0.010 \pm 0.003\,, \end{aligned}$$

with a χ^2/NDOF=75.8/109. The central values and the first errors of $M_{\rm t}$ and $\alpha_s(M_{\rm Z}^2)$ refer to a fixed value of $M_{\rm H} = 300$ GeV. The second error shows the variation of the central value for Higgs masses spanning the interval $60 < M_{\rm H}({\rm GeV}) < 1000$. In the context of the Standard Model our measurements lead to a value of $M_{\rm W} = 80.05^{+0.24}_{-0.26}$ GeV for $M_{\rm H} = 300$ GeV. The change of this value for $M_{\rm W}$ is negligible for Higgs masses in the range $60 < M_{\rm H}\,({\rm GeV}) < 1000$. Our result for $M_{\rm W}$ is in good agreement with the direct measurements of CDF and UA2 [18] and of similar precision. The fitted value for $\alpha_s(M_{\rm Z}^2)$ is essentially determined from the ratio $R_\ell = \Gamma_{\rm had}/\Gamma_{\ell\ell}$ and the total width $\Gamma_{\rm Z}$. The value we obtain is consistent with the OPAL values [19], $\alpha_s(M_{\rm Z}^2) = 0.122^{+0.005}_{-0.006}$, determined from event topologies, jet rates and energy correlations and, $\alpha_s(M_{\rm Z}^2) = 0.123^{+0.006}_{-0.007}$, determined from τ decays. If we calculate $\alpha_s(M_{\rm Z}^2)$ from R_ℓ alone, we obtain for $M_{\rm t}$=150 GeV and $M_{\rm H}$=300 GeV, $\alpha_s(M_{\rm Z}^2) = 0.134 \pm 0.013({\rm exp.})^{+0.003}_{-0.002}(M_{\rm t}) \pm 0.002(M_{\rm H})$ where the second and third errors reflect the variation of our result for the $M_{\rm t}$ and $M_{\rm H}$ ranges quoted above.

Figures 8 and 9 show comparisons of the measured cross sections and asymmetries with the result of the Standard Model fit. We observe excellent agreement between the data and the result of the fit.

Figure 10 shows the χ^2-curves, as a function of $M_{\rm t}$, for the direct Standard Model fit to the corrected cross sections and forward-backward asymmetries. From these χ^2-curves we derive an upper limit on $M_{\rm t}$ of:

$$M_{\rm t} < 210\,{\rm GeV}\ \ {\rm at}\ \ 95\%\ {\rm CL}\,.$$

7.4 Epsilon Parameter Fits

In this section we analyse our data in terms of parameters which are aimed at decoupling the effects of unknown top and Higgs masses from the possible effects of new physics. We use the 'ϵ' parameters [20] defined in terms of the vector and axial-vector couplings. Allowing for electroweak corrections, $\hat{g}_v^\ell$ and $\hat{g}_a^\ell$ may be written as:

$$\hat{g}_a^\ell = \sqrt{1+\Delta\rho} I_3 \quad (1)$$

$$\hat{g}_v^\ell = \sqrt{1+\Delta\rho}\left[I_3 - 2Q_f s_0^2(1+\Delta k)\right] . \quad (2)$$

Here I_3 refers to the weak isospin of charged leptons and $s_0^2 = 1 - c_0^2 = 0.2313 \pm 0.0003$ [16] refers to an effective mixing angle after only pure QED corrections. The quoted error for s_0 is due to the uncertainty in the contribution of light quarks to the photon vacuum polarization [21]. The parameters $\Delta\rho$ and Δk contain most of the $M_{\rm t}$ and $M_{\rm H}$ dependence. It is well documented that [17, 21]:

$$\Delta\rho \approx -\frac{(c_0^2 - s_0^2)}{c_0^2}\Delta k \approx \frac{3G_{\rm F}}{8\pi^2\sqrt{2}} M_{\rm t}^2 \quad (3)$$

The parameters ϵ_1 and ϵ_3 are then defined by:

$$\hat{g}_a^\ell = \sqrt{1+\epsilon_1} I_3 \quad (4)$$

$$\hat{g}_v^\ell = \sqrt{1+\epsilon_1}\left[I_3 - 2Q_f s_0^2 + 2Q_f \frac{c_0^2 s_0^2}{c_0^2 - s_0^2}\left(\epsilon_1 - \frac{\epsilon_3}{c_0^2}\right)\right] . \quad (5)$$

The result of this is that $\epsilon_1 \equiv \Delta\rho$ contains most of the $M_{\rm t}$ and $M_{\rm H}$ dependence. The parameter ϵ_3, however, is largely free from such effects. A measurement of ϵ_3 is therefore an unambiguous test of the Standard Model, and has the potential to disentangle the effects of some classes of new physics.

In the following we present three such fits based upon the results of our model independent fit in Table 8, column 3:

- Fit 1 uses only the parameters $C_{\rm ZZ}^s$ and $C_{\rm ZZ}^a$ which correspond to the defining measurements for ϵ_1 and ϵ_3, namely $\Gamma_{\ell\ell}$ and $A_{\rm FB}^{\rm pole}$.
- Fit 2 uses all C parameters
- Fit 3 uses also the information contained in $\Gamma_{\rm Z}$ and $\sigma_{\rm had}^{\rm pole}$. We incorporate them in such a way as to eliminate the effect of complications arising from QCD and the b-quark vertex. This is achieved by fitting to the expression:

$$\Gamma_{\rm Z}^{\rm meas} = \Gamma_{\rm had}^{\rm meas} + (3+\delta_m)\Gamma_{\ell\ell} + 3\left(\frac{\Gamma_{\nu\nu}}{\Gamma_{\ell\ell}}\right)_{\rm SM}\Gamma_{\ell\ell} . \quad (6)$$

  $\Gamma_{\rm had}$ is itself derived from a parameter transformation on $\sigma_{\rm had}^{\rm pole}$ (as described in [1]), leaving an expression which contains measured quantities, which are varied within their error, and $\Gamma_{\ell\ell}$ as the only quantity parametrized in terms of $\hat{g}_v^\ell\,(\epsilon_1,\epsilon_3)$ and $\hat{g}_a^\ell\,(\epsilon_1,\epsilon_3)$.

The results of these three fits are summarized in Table 11. The values obtained for ϵ_1 and ϵ_3 in Fits 1–3 are compatible with each other. Figure 11 displays the one standard deviation contours in the ϵ_1-ϵ_3 plane from Fit 3. The comparison with a range of Standard Model values is also indicated in Figure 11 and shows good agreement.

8 Summary and Conclusions

We have presented an update to our published results by adding a total of 733 059 $e^+e^- \to$ hadrons, 25 280 $e^+e^- \to e^+e^-$, 34 259 $e^+e^- \to \mu^+\mu^-$ and 28 553 $e^+e^- \to \tau^+\tau^-$ events, recorded during 1992 at a mean centre-of-mass energy of 91.299 GeV. The results are consistent with our previous publication, and the precision of parameters such as R_ℓ and $A_{\rm FB}^{\rm pole}$, where the errors are dominated by the number of leptonic events at $\sqrt{s} = M_{\rm Z}^2$, has improved significantly.

We have performed a model independent analysis of Z^0 parameters based on an extension of the improved Born approximation. We have also performed a model independent test for new physics based on the framework suggested in [20]. Comparing the resulting parameters with the Standard Model prediction we observe good agreement. Several observables that test lepton universality have been presented and show agreement with this hypothesis.

From a fit of the Standard Model prediction to our data we determine

$$M_{\rm t} = 132^{+41\ +24}_{-48\ -18}\ \text{GeV}$$

and

$$\alpha_s(M_{\rm Z}^2) = 0.124 \pm 0.010 \pm 0.003\,,$$

where the central values and the first errors of $M_{\rm t}$ and $\alpha_s(M_{\rm Z}^2)$ refer to a fixed value of $M_{\rm H} = 300$ GeV and the second errors show the variation of the central value for Higgs masses spanning the interval $60 < M_{\rm H}\,(\text{GeV}) < 1000$. The strong coupling constant determined from this fit is in good agreement with results derived from event topologies, jet rates, energy correlations and τ decays.

Our results are consistent with those of the other LEP Collaborations [22].

Acknowledgements

We are grateful to D. Bardin, W. Beenakker, F.A. Berends, M. Bilenky, S. Jadach, R. Kleiss, J.H. Kühn, S.C. van der Marck, T. Riemann, M. Sachwitz and Z. Wąs for their help and advice concerning the programs and the analytic formulae used in this analysis.

It is a pleasure to thank the SL Division for the efficient operation of the LEP accelerator, the precise information on the absolute energy, and their continuing close cooperation with our experimental group. In addition to the support staff at our own institutions we are pleased to acknowledge the
Department of Energy, USA,
National Science Foundation, USA,
Texas National Research Laboratory Commission, USA,
Science and Engineering Research Council, UK,
Natural Sciences and Engineering Research Council, Canada,
Fussefeld Foundation,
Israeli Ministry of Energy and Ministry of Science,
Minerva Gesellschaft,
Japanese Ministry of Education, Science and Culture (the Monbusho) and a grant under the Monbusho International Science Research Program,
German Israeli Bi-national Science Foundation (GIF),
Direction des Sciences de la Matière du Commissariat à l'Energie Atomique, France,
Bundesministerium für Forschung und Technologie, Germany,
National Research Council of Canada,
A.P. Sloan Foundation and Junta Nacional de Investigação Científica e Tecnológica, Portugal.

Source of Uncertainty	Uncertainty '92
8 'Telescope' study	0.17 %
drift chamber survey of tubes	0.17 %
simulation systematics	0.23 %
locations of drift chamber sense wires	0.08 %
distance to interaction point	0.04 %
calorimeter coordinates	<0.01 %
trigger inefficiency	<0.02 %
reconstruction inefficiency	<0.01 %
accidental background	<0.01 %
data statistics	0.18 %
Monte Carlo statistics	0.12 %
overall	**0.41 %**

Table 1: Summary of experimental uncertainties in the 1992 absolute luminosity analysis.

	Correction Factor f	Uncertainty $\Delta f/f$ [%]
Acceptance/Efficiency:		
$e^+e^- \to$ hadrons Monte Carlo	1.0048	0.04
quality of detector simulation	1.0000	0.14
failures in data acquisition / reconstruction	1.0000	0.04
Background:		
$e^+e^- \to \tau^+\tau^-$	0.9983	0.01
non-resonant background (0.060 ± 0.016 nb)	0.9980	0.05
forward detector accidental hits	1.0000	0.05
Theoretical error:		
fragmentation	1.0000	0.11
overall	**1.0011**	**0.20**

Table 2: Summary of the correction factors and systematic errors for the 1992 hadronic cross section calculation. The uncertainty of the non-resonant background of 0.016 nb is treated as correlated with off-peak data points from earlier data.

	Correction Factor f	Uncertainty $\Delta f/f$ [%]
Acceptance/Efficiency:		
edge of acceptance	1.0000	0.12
calorimeter energy cut	1.0036	0.11
track inefficiency	1.0049	0.09
multiplicity cut	1.0001	0.01
trigger efficiency	1.0000	$<<$0.01
Background:		
$e^+e^- \to \tau^+\tau^-$	0.9962	0.11
$e^+e^- \to$ hadrons	0.9998	0.02
$e^+e^- \to \gamma\gamma$	0.9999	0.02
$e^+e^- \to e^+e^-e^+e^-$	1.0000	$<$0.02
overall	**1.0045**	**0.22**

Table 3: Summary of the correction factors and systematic errors for the 1992 $e^+e^- \to e^+e^-$ cross section calculation. The correction factors listed apply to the restricted angular ranges of $|\cos\theta| < 0.70$ and acollinearity $< 10^\circ$ used for this analysis.

	Correction Factor f	Uncertainty $\Delta f/f$ [%]
Acceptance/Efficiency:		
$e^+e^- \to \mu^+\mu^-$ Monte Carlo	1.0942	0.07
tracking losses	1.0048	0.10
muon identification	1.0003	0.05
edge of geometrical acceptance	1.0000	0.05
cut on number of tracks	1.0000	0.05
only one final-state photon in KORALZ	1.0000	0.05
trigger efficiency	1.0010	0.02
treatment of four-fermion events	1.0004	0.02
online filter efficiency	1.0000	0.02
Background:		
$e^+e^- \to \tau^+\tau^-$	0.9904	0.10
cosmic rays	0.9997	0.02
$e^+e^- \to e^+e^-\mu^+\mu^-$	0.9999	0.01
overall	**1.0903**	**0.19**

Table 4: Summary of the correction factors and systematic errors for the 1992 $e^+e^- \to \mu^+\mu^-$ cross section calculation. Note that the effects 'muon identification', 'tracking losses' and 'cut on number of tracks' were, in principle, simulated by the Monte Carlo. The quoted corrections were introduced to take into account the observed discrepancies between the data and Monte Carlo for these effects.

	Correction Factor f	Uncertainty $\Delta f/f$ [%]
Acceptance/Efficiency:		
$e^+e^- \to \tau^+\tau^-$ Monte Carlo	1.3299	0.13
τ-pair selection cuts	1.0000	0.26
definition of $\|\cos\theta\|$	1.0000	0.17
vertex cut	1.0003	0.02
treatment of four-fermion events	1.0000	0.03
time-of-flight efficiency	1.0011	0.02
trigger efficiency	1.0008	0.08
uncertainty of tau branching fraction	1.0000	<0.05
misclassification as e^+e^-	1.0012	0.06
misclassification as $\mu^+\mu^-$	1.0000	0.08
Background:		
$e^+e^- \to$ hadrons	0.9949	0.14
$e^+e^- \to e^+e^-$	0.9959	0.15
$e^+e^- \to \mu^+\mu^-$	0.9902	0.11
cosmic rays and beam-gas events	0.9995	0.05
two-photon reactions	0.9953	0.05
overall	**1.3024**	**0.44**

Table 5: Summary of the correction factors and systematic errors for the 1992 $e^+e^- \to \tau^+\tau^-$ cross section calculation. Note that the losses of events due to misclassification as e^+e^- and $\mu^+\mu^-$ events were, in principle, simulated by the Monte Carlo. The quoted corrections were introduced to take into account the observed discrepancies between the data and Monte Carlo.

$\sqrt{s}$ (GeV)	$\sigma_{\rm had}^{\rm tot}$ (nb)	σ_{ee} (nb)	$\sigma_{\mu\mu}^{\rm tot}$ (nb)	$\sigma_{\tau\tau}^{\rm tot}$ (nb)
91.299	30.707±0.045	1.0108±0.0065	1.4846±0.0083	1.4786±0.0090

Table 6: The 1992 cross sections without systematic errors, from a total of 733 059 $e^+e^- \to$ hadrons events, 23 998 $e^+e^- \to e^+e^-$ events, 32 492 $e^+e^- \to \mu^+\mu^-$ events and 27 036 $e^+e^- \to \tau^+\tau^-$ events. The cross sections are quoted including the statistical uncertainty of luminosity Bhabha events. $\sigma_{\rm had}^{\rm tot}$ is the total cross section after correction for efficiency and acceptance. σ_{ee} is the cross section measured within the angular acceptance $|\cos\theta| < 0.70$ and the acollinearity angle less than 10°, corrected for the effects of efficiency. $\sigma_{\mu\mu}^{\rm tot}$ and $\sigma_{\tau\tau}^{\rm tot}$ are the total cross sections after correction for efficiency and acceptance for a cut on the mass of the final state fermion pair $\sqrt{s'} > 0.1\sqrt{s}$.

	cuts				A_{FB}	A_{FB}	exp. syst.
	$\|\cos\theta\|$	acol.	N_F	N_B	(Counting)	(Fitting)	error
e^+e^-	0.70	10°	13885	11395	0.0988±0.0063	–	0.002
$\mu^+\mu^-$	0.95	15°	16937	16527	0.0123±0.0055	0.0084±0.0051	0.001
$\tau^+\tau^-$	0.90	15°	14259	13778	0.0162±0.0060	0.0166±0.0056	0.002

Table 7: The 1992 leptonic forward-backward asymmetries at $\sqrt{s} = 91.299$ GeV within the angular acceptance cuts given in columns 2 and 3. The forward-backward asymmetries in column 6 were obtained from the numbers in columns 4 and 5 corrected for background and efficiency; column 7 lists the results from maximum likelihood fits to the $\cos\theta$ distributions. In columns 6 and 7 only statistical errors are quoted. The experimental systematic errors, given in column 8, are assumed to be uncorrelated among the different lepton species.

Improved Born Approximation Equivalent	Without Lepton Universality	With Lepton Universality
$C^s_{\rm ZZ}(e^+e^-) \equiv (\hat{g}_a^{e\,2} + \hat{g}_v^{e\,2})(\hat{g}_a^{e\,2} + \hat{g}_v^{e\,2})$	0.06335±0.00080	
$C^s_{\rm ZZ}(\mu^+\mu^-) \equiv (\hat{g}_a^{e\,2} + \hat{g}_v^{e\,2})(\hat{g}_a^{\mu\,2} + \hat{g}_v^{\mu\,2})$	0.06350±0.00071	
$C^s_{\rm ZZ}(\tau^+\tau^-) \equiv (\hat{g}_a^{e\,2} + \hat{g}_v^{e\,2})(\hat{g}_a^{\tau\,2} + \hat{g}_v^{\tau\,2})$	0.06294±0.00077	
$C^s_{\rm ZZ}(\ell^+\ell^-) \equiv (\hat{g}_a^{\ell\,2} + \hat{g}_v^{\ell\,2})^2$		0.06326±0.00067
$C^a_{\rm ZZ}(e^+e^-) \equiv \hat{g}_a^e\ \hat{g}_v^e\ \hat{g}_a^e\ \hat{g}_v^e$	0.00013±0.00017	
$C^a_{\rm ZZ}(\mu^+\mu^-) \equiv \hat{g}_a^e\ \hat{g}_v^e\ \hat{g}_a^\mu\ \hat{g}_v^\mu$	0.000213±0.000094	
$C^a_{\rm ZZ}(\tau^+\tau^-) \equiv \hat{g}_a^e\ \hat{g}_v^e\ \hat{g}_a^\tau\ \hat{g}_v^\tau$	0.00043±0.00011	
$C^a_{\rm ZZ}(\ell^+\ell^-) \equiv (\hat{g}_a^\ell\ \hat{g}_v^\ell)^2$		0.000272±0.000066
$C^a_{\gamma\rm Z}(e^+e^-) \equiv \hat{g}_a^e\ \hat{g}_a^e$	0.178±0.051	
$C^a_{\gamma\rm Z}(\mu^+\mu^-) \equiv \hat{g}_a^e\ \hat{g}_a^\mu$	0.211±0.027	
$C^a_{\gamma\rm Z}(\tau^+\tau^-) \equiv \hat{g}_a^e\ \hat{g}_a^\tau$	0.230±0.028	
$C^a_{\gamma\rm Z}(\ell^+\ell^-) \equiv \hat{g}_a^{\ell\,2}$		0.217±0.018
$C^s_{\gamma\rm Z}(e^+e^-) \equiv \hat{g}_v^e\ \hat{g}_v^e$	-0.029±0.034	
$C^s_{\gamma\rm Z}(\mu^+\mu^-) \equiv \hat{g}_v^e\ \hat{g}_v^\mu$	0.017±0.022	
$C^s_{\gamma\rm Z}(\tau^+\tau^-) \equiv \hat{g}_v^e\ \hat{g}_v^\tau$	0.029±0.024	
$C^s_{\gamma\rm Z}(\ell^+\ell^-) \equiv \hat{g}_v^{\ell\,2}$		0.014±0.015
$M_{\rm Z}$ [GeV]	91.182±0.007±0.006	91.181±0.007±0.006
$\Gamma_{\rm Z}$ [GeV]	2.483±0.011±0.004	2.482±0.011±0.004
$\sigma^{\rm pole}_{\rm had}$ [nb]	41.71±0.23	41.70±0.23
χ^2/NDOF	63.3/97	70.0/105

Table 8: Results of the model-independent fits to the leptonic cross sections and forward-backward asymmetries. The hadronic cross section measurements are also included in both fits. The values obtained for χ^2 in the parameter fits are dominated by the size of the statistical errors. When the fits were repeated with the values of systematic errors set to zero, the resulting χ^2 values were 75.5 and 84.2 for the fits in columns 2 and 3, respectively.

Without Lepton Universality:	
Γ_{ee}	83.63±0.53
$\Gamma_{\mu\mu}$	83.83±0.65
$\Gamma_{\tau\tau}$	82.90±0.77
$\Gamma_{\rm had}$	1742±11
With Lepton Universality:	
$\Gamma_{\ell\ell}$	83.55±0.44
$\Gamma_{\rm had}$	1741±10

Table 9: Z^0 partial decay widths [MeV] obtained by a parameter transformation from M_Z, Γ_Z, $\sigma_{\rm had}^{\rm pole}$ and the C_{ZZ}^s parameters in Table 8.

	Without Lepton Universality	With Lepton Universality	SM Prediction
R_e	20.83±0.16		
R_μ	20.78±0.11		
R_τ	21.01±0.15		
R_ℓ		20.835±0.086	$20.75^{+0.02}_{-0.03}$
$A_{FB}^{\rm pole}(e^+e^-)$	0.0062±0.0080		
$A_{FB}^{\rm pole}(\mu^+\mu^-)$	0.0099±0.0042		
$A_{FB}^{\rm pole}(\tau^+\tau^-)$	0.0205±0.0052		
$A_{FB}^{\rm pole}$		0.0128±0.0030	$0.014^{+0.006}_{-0.003}$
M_Z [GeV]	91.182±0.007±0.006	91.181±0.007±0.006	input
Γ_Z [GeV]	2.483±0.011±0.004	2.482±0.011±0.004	$2.489^{+0.022}_{-0.018}$
$\sigma_{\rm had}^{\rm pole}$ [nb]	41.71±0.23	41.70±0.23	$41.46^{+0.06}_{-0.03}$

Table 10: Results of a parameter transformation from M_Z, Γ_Z, $\sigma_{\rm had}^{\rm pole}$ and the C_{ZZ}^s parameters in Table 8 into the standard LEP parameter set. The second error quoted on M_Z and Γ_Z is due to the uncertainty of the LEP energy. In the last column we give the Standard Model value for each parameter assuming $M_t = 150$ GeV, $M_H = 300$ GeV and $\alpha_s(M_Z^2) = 0.12$, fixed. The range quoted for the Standard Model prediction reflects variations of M_t in the interval $50 < M_t\,({\rm GeV}) < 230$ and M_H in the interval $60 < M_H\,({\rm GeV}) < 1000$.

	$\epsilon_1 \cdot 10^3$	$\epsilon_3 \cdot 10^3$	χ^2/NDOF
Fit 1	1.7 ± 5.4	6.4 ± 6.7	0/0
Fit 2	1.4 ± 5.3	4.6 ± 6.5	4/2
Fit 3	-0.5 ± 5.1	2.8 ± 6.3	6/3

Table 11: ϵ parameters obtained by the fits described in the text to M_Z, Γ_Z, $\sigma_{\rm had}^{\rm pole}$ and the C parameters in Table 8.

A Appendix: Correlation Matrices

Parameter		1	2	3	4	5
1	M_{Z}	1.000	.001	.007	.057	.066
2	Γ_{Z}	.001	1.000	-.089	.036	.015
3	$\sigma_{\mathrm{had}}^{\mathrm{pole}}$	.007	-.089	1.000	.222	.017
4	R_ℓ	.057	.036	.222	1.000	.010
5	$A_{\mathrm{FB}}^{\mathrm{pole}}$	.066	.015	.017	.010	1.000

Table 12: The parameter correlation matrix for the standard LEP parametrization assuming lepton universality. The results of this fit are summarized in Table 10 column 3.

Parameter		1	2	3	4	5	6	7	8	9
1	M_{Z}	1.000	.003	-.014	.169	-.008	-.012	-.081	.080	.077
2	Γ_{Z}	.003	1.000	-.089	.022	.035	.012	-.004	.010	.017
3	$\sigma_{\mathrm{had}}^{\mathrm{pole}}$	-.014	-.089	1.000	.042	.195	.147	.087	-.019	-.013
4	R_{e}	.169	.022	.042	1.000	.135	.079	-.165	.075	.065
5	R_μ	-.008	.035	.195	.135	1.000	.099	.004	.004	-.003
6	R_τ	-.012	.012	.147	.079	.099	1.000	.008	-.007	.000
7	$A_{\mathrm{FB}}^{\mathrm{pole}}(\mathrm{e^+e^-})$	-.081	-.004	.087	-.165	.004	.008	1.000	-.040	-.035
8	$A_{\mathrm{FB}}^{\mathrm{pole}}(\mu^+\mu^-)$	.080	.010	-.019	.075	.004	-.007	-.040	1.000	.035
9	$A_{\mathrm{FB}}^{\mathrm{pole}}(\tau^+\tau^-)$	.077	.017	-.013	.065	-.003	.000	-.035	.035	1.000

Table 13: The parameter correlation matrix for the standard LEP parametrization without assuming lepton universality. The results of this fit are summarized in Table 10 column 2.

Parameter		1	2	3	4	5	6	7
1	M_{Z}	1.000	.009	-.065	.000	.000	.064	-.162
2	$\sigma_{\mathrm{had}}^{\mathrm{pole}}$	.009	1.000	.350	-.090	.040	.041	-.018
3	C_{ZZ}^s	-.065	.350	1.000	.817	.113	.094	.078
4	Γ_{Z}	.000	-.090	.817	1.000	.099	.082	.022
5	$C_{\gamma\mathrm{Z}}^a$	.000	.040	.113	.099	1.000	.184	-.046
6	C_{ZZ}^a	.064	.041	.094	.082	.184	1.000	.008
7	$C_{\gamma\mathrm{Z}}^s$	-.162	-.018	.078	.022	-.046	.008	1.000

Table 14: The parameter correlation matrix for the extended effective Born approach assuming lepton universality. The results of this fit are summarized in Table 8 column 3.

Parameter		1	2	3	4	5	6	7	8	9	10	11	12	13	14	15
1	M_{Z}	1.000	-.010	-.144	-.049	-.041	-.001	-.004	.009	.009	-.083	.077	.074	-.073	-.112	-.096
2	$\sigma_{\mathrm{had}}^{\mathrm{pole}}$	-.010	1.000	.347	.330	.302	-.083	-.026	.029	.032	.088	-.004	.008	-.056	-.001	.001
3	$C_{\mathrm{ZZ}}^{s}(\mathrm{e^+e^-})$	-.144	.347	1.000	.742	.678	.690	-.027	.060	.062	.143	-.015	.011	.024	.038	.041
4	$C_{\mathrm{ZZ}}^{s}(\mu^+\mu^-)$	-.049	.330	.742	1.000	.730	.781	-.011	.075	.071	.049	.038	.054	-.040	.112	.031
5	$C_{\mathrm{ZZ}}^{s}(\tau^+\tau^-)$	-.041	.302	.678	.730	1.000	.723	-.010	.062	.088	.042	.031	.072	-.036	.022	.116
6	Γ_{Z}	-.001	-.083	.690	.781	.723	1.000	.002	.067	.069	.004	.044	.065	-.021	.023	.030
7	$C_{\gamma\mathrm{Z}}^{a}(\mathrm{e^+e^-})$	-.004	-.026	-.027	-.011	-.010	.002	1.000	-.001	-.001	.068	.002	.001	.196	.000	.000
8	$C_{\gamma\mathrm{Z}}^{a}(\mu^+\mu^-)$	.009	.029	.060	.075	.062	.067	-.001	1.000	.006	.001	.199	.007	-.005	-.101	.001
9	$C_{\gamma\mathrm{Z}}^{a}(\tau^+\tau^-)$	.009	.032	.062	.071	.088	.069	-.001	.006	1.000	.001	.006	.191	-.006	-.001	-.123
10	$C_{\mathrm{ZZ}}^{a}(\mathrm{e^+e^-})$	-.083	.088	.143	.049	.042	.004	.068	.001	.001	1.000	-.038	-.032	.006	.015	.013
11	$C_{\mathrm{ZZ}}^{a}(\mu^+\mu^-)$	.077	-.004	-.015	.038	.031	.044	.002	.199	.006	-.038	1.000	.036	-.009	.005	-.011
12	$C_{\mathrm{ZZ}}^{a}(\tau^+\tau^-)$	.074	.008	.011	.054	.072	.065	.001	.007	.191	-.032	.036	1.000	-.010	-.012	.009
13	$C_{\gamma\mathrm{Z}}^{s}(\mathrm{e^+e^-})$	-.073	-.056	.024	-.040	-.036	-.021	.196	-.005	-.006	.006	-.009	-.010	1.000	.028	.024
14	$C_{\gamma\mathrm{Z}}^{s}(\mu^+\mu^-)$	-.112	-.001	.038	.112	.022	.023	.000	-.101	-.001	.015	.005	-.012	.028	1.000	.038
15	$C_{\gamma\mathrm{Z}}^{s}(\tau^+\tau^-)$	-.096	.001	.041	.031	.116	.030	.000	.001	-.123	.013	-.011	.009	.024	.038	1.000

Table 15: The parameter correlation matrix for the extended effective Born approach without assuming lepton universality. The results of this fit are summarized in Table 8 column 2.

References

[1] OPAL Collaboration, P.D. Acton et al., Z. Phys. **C58** (1993) 219.

[2] OPAL Collaboration, G. Alexander et al., Z. Phys. **C52** (1991) 175.

[3] OPAL Collaboration, K. Ahmet et al., Nucl. Inst. Meth. **A305** (1991) 275.

[4] JETSET, Version 7.3; T. Sjöstrand, Comp. Phys. Comm. **39** (1986) 347;
T. Sjöstrand and M. Bengtsson, Comp. Phys. Comm. **43** (1987) 367;
T. Sjöstrand, CERN-TH/6488/92.

[5] HERWIG, Version 5.5; G. Marchesini and B.R. Webber, Nucl. Phys. **B310** (1988) 461;
G. Marchesini et al., Comp. Phys. Comm. **67** (1992) 465.

[6] OPAL Collaboration, M.Z. Akrawy et al., Z. Phys. **C47** (1990) 505; OPAL Collaboration, P.D. Acton et al., Z. Phys. **C58** (1993) 387.

[7] S. Jadach et al., Comp. Phys. Comm. **66** (1991) 276.

[8] M. Böhm, A. Denner and W. Hollik, Nucl. Phys. **B304** (1988) 687;
F. A. Berends, R Kleiss, W. Hollik, Nucl. Phys. **B304** (1988), 712.

[9] S. Jadach et al., Comp. Phys. Comm. **70** (1992) 305.

[10] J. Allison et al., Nucl. Inst. Meth. **A317** (1992) 47.

[11] B.E. Anderson et al., Nucl. Inst. Meth., **A283** (1989) 650;
D.C. Imrie et al. Nucl. Inst. Meth. **A283** (1989) 515.

[12] R. Brun et al., GEANT 3, Report DD/EE/84-1, CERN (1989).

[13] W. Beenakker et al., Nucl. Phys. **B349** (1991) 323.

[14] 'The Energy Calibration of LEP in 1991', L. Arnaudon et al., CERN-PPE/92-125 and CERN-SL/92-37(DI);
Working group on LEP energy and the LEP Collaborations, Phys. Lett. **B307** (1993) 187.

[15] 'The Energy Calibration of LEP in 1992', L. Arnaudon et al., CERN SL/93-21 (DI), April 1993

[16] Line shape program ZFITTER, version 4.6, Dubna-Zeuthen radiative correction group;
D. Bardin et al., Comp. Phys. Comm. **59** (1990) 303; Z. Phys. **C44** (1989) 493; Nucl. Phys. **B351** (1991) 1; Phys. Lett. **B229** (1989) 405; CERN-TH 6443/92 (May 1992).

[17] M. Consoli and W. Hollik, Proceedings of the Workshop on Z Physics at LEP1, CERN 89-08, Sept. 1989, ed. G. Altarelli et al., Vol 1 (1989) 7.

[18] CDF Collaboration, F. Abe et al., Phys. Rev. Lett. **65** (1990) 2243; Phys. Rev. **D43** (1991) 2070;
UA2 Collaboration, J. Alitti et al., Phys. Lett. **B276** (1992) 354.

[19] OPAL Collaboration, P.D. Acton et al., Z. Phys. **C55** (1992) 1.

[20] G. Altarelli, R. Barbieri and F. Caravaglios, CERN TH 6770-93. G. Altarelli, R. Barbieri and F. Caravaglios, CERN TH 6859-93. G. Altarelli, R. Barbieri and S. Jadach, Nucl. Phys. **B369** (1992) 3; E: Nucl. Phys. **B376** (1992) 444.

[21] G. Burgers et al., Proceedings of the Workshop on Z Physics at LEP1, CERN 89-08, Sept. 1989, ed. G. Altarelli et al., Vol 1 (1989) 55.

[22] ALEPH Collaboration, D. Decamp et al., Z. Phys. **C53** (1992) 1;
DELPHI Collaboration, P. Abreu et al., Nucl. Phys. **B367** (1991) 511;
L3 Collaboration, B. Adeva et al., Z. Phys. **C51** (1991) 179;
The LEP Collaborations: ALEPH, DELPHI, L3 and OPAL, Phys. Lett. **B276** (1992) 247;
ALEPH Collaboration, D. Buskulik et al., CERN-PPE/93-40;
L3 Collaboration, O. Adriani et al., CERN-PPE/93-31.

Figure Captions

Figure 1: Fraction of luminosity observed in 8 different telescopes defined by dividing the Bhabha acceptance in ϕ. The non-statistical structure seen in the figure is due to local inhomogeneities in the tube chamber reconstruction.

Figure 2: $e^+e^- \to e^+e^-$ selection: The points represent the data, the unshaded area is the electron pair Monte Carlo and the hatched area is the background simulaton. The arrow indicates the cut value. (a) Distribution of the sum of electromagnetic energy after all other cuts in the angular range $|\cos\theta| < 0.70$. (b) Acoplanarity distribution of events with the total electromagnetic energy satisfying $(0.7 < \Sigma E_{clust}/\sqrt{s} < 0.8)$. (c) Distribution of the sum of the charged track momenta, normalized to the centre of mass energy, for the events with small acoplanarity ($< 0.2^\circ$) and low electromagnetic energy $(0.5 < \Sigma E_{clust}/\sqrt{s} < 0.8)$. The peak near $\Sigma E_{clust}/\sqrt{s} = 1$ indicates the existence of e^+e^- events.

Figure 3: Measured angular distribution of $e^+e^- \to e^+e^-$ events within $|\cos\theta| < 0.90$, compared with ALIBABA calculation (the curve). The data were corrected for inefficiency and backgrounds. The parameters used in the ALIBABA calculation were: $M_{\rm Z} = 91.181$ GeV, $M_{\rm t} = 150$ GeV and $M_{\rm H} = 300$ GeV.

Figure 4: $e^+e^- \to \mu^+\mu^-$ selection: Comparison of the visible energy fraction for data and Monte Carlo events in the tau pair background studies. The points represent the combined 1991 and 1992 data. The unshaded area is the muon pair Monte Carlo, the singly hatched area is the tau pair Monte Carlo, and the cross-hatched area is the two-photon Monte Carlo. The region between the arrows was considered in the systematic analysis. (a) Distributions for events in the tau-enriched muon pair sample. (b) Distributions for events in the electron-muon tau pair sample.

Figure 5: $e^+e^- \to \tau^+\tau^-$ selection: The total shower energy fraction after all the selection cuts except for the shower energy cut. a) No additional cuts are made. b) Require at least one of the τ jets to have a momentum less than 40% of the beam energy and in addition, require the acoplanarity angle to be greater than 0.5^0. c) The higher shower energy region of distribution b).
The open area shows the Monte Carlo distribution for the process $e^+e^- \to \tau^+\tau^-$. The shaded area shows the Monte Carlo distribution for background events only (mostly $e^+e^- \to e^+e^-$).

Figure 6: Comparison of the parameters from the model independent fit (Table 8 column 3) with the Standard Model prediction as a function of $M_{\rm t}$. The cross-hatched area shows the variation of the Standard Model prediction with $M_{\rm H}$ spanning the interval $60 < M_{\rm H}\,({\rm GeV}) < 1000$ and the singly-hatched area corresponds to a variation of $\alpha_s(M_{\rm Z}^2)$ within the interval $0.11 < \alpha_s(M_{\rm Z}^2) < 0.13$. The experimental errors on the parameters are indicated as vertical bands.

Figure 7: One standard deviation contours (39% probability content) in the R_ℓ-$A_{\rm FB}^{\rm pole}$ plane for each leptonic species and for all leptons assuming lepton universality. The shaded area is the Standard Model prediction for $50 < M_{\rm t}\,({\rm GeV}) < 230$ and $60 < M_{\rm H}\,({\rm GeV}) < 1000$.

Figure 8: Cross sections as functions of centre-of-mass energy for:
a) $e^+e^- \to$ hadrons, corrected for acceptance;
b) $e^+e^- \to e^+e^-$, integrated over $|\cos\theta| < 0.70$ and corrected for efficiency within the geometrical acceptance;
c) $e^+e^- \to \mu^+\mu^-$, corrected for acceptance;
d) $e^+e^- \to \tau^+\tau^-$, corrected for acceptance.
The solid lines are the results of the fit to the combined e^+e^-, $\mu^+\mu^-$, $\tau^+\tau^-$ and hadronic data described in the text. The solid squares show the 1992 data, the solid circles the 1991 data and the open circles the 1990 data. The data are corrected for the centre-of-mass energy spread. The lower plots display the residuals to the Standard Model fit. Only statistical errors are shown.

Figure 9: Forward-backward asymmetries for:
a) $e^+e^- \to e^+e^-$, within $|\cos\theta| < 0.70$;
b) $e^+e^- \to \mu^+\mu^-$, within $|\cos\theta| < 0.95$;
c) $e^+e^- \to \tau^+\tau^-$, within $|\cos\theta| < 0.90$.
d) The difference averaged over all 3 leptonic species between the measured forward-backward asymmetry and the Standard Model fit result.
The solid lines are the results of the fit to the combined e^+e^-, $\mu^+\mu^-$, $\tau^+\tau^-$ and hadronic data described in the text. The solid squares show the 1992 data, the solid circles the 1991 data and the open circles the 1990 data. The data are corrected for the centre-of-mass energy spread. Only statistical errors are shown.

Figure 10: The χ^2 curves for the fit to $M_{\rm t}$ and $\alpha_s(M_{\rm Z}^2)$, using the OPAL cross section and forward-backward asymmetry measurements, for three different Higgs mass values spanning the interval $60 < M_{\rm H}\,({\rm GeV}) < 1000$. The minimum value of χ^2 from the $M_{\rm H} = 60$ GeV curve has been subtracted from all curves. In these fits the strong coupling constant is unconstrained.

Figure 11: One standard deviation contours (39% probability content) in the ϵ_1-ϵ_3 plane for a fit to line shape and lepton asymmetry data. Also indicated is the Standard Model prediction for the ϵ parameters. The symbols refer to $M_{\rm t} = 90$ GeV, 150 GeV and 200 GeV, where the symbol size increases with $M_{\rm t}$. Circular, box and triangular symbols discriminate between $M_{\rm H} = 60$ GeV, 300 GeV and 1000 GeV, respectively.

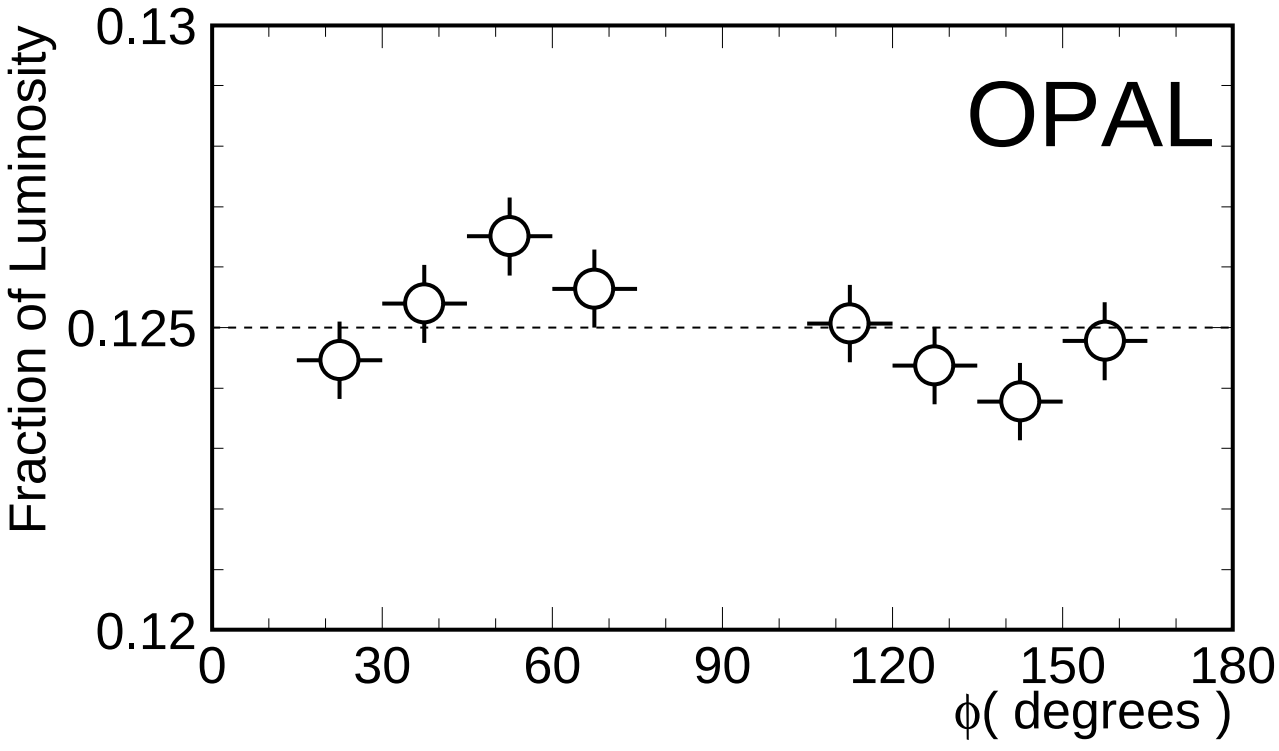
OPAL
Fraction of Luminosity
0.13
0.125
0.12
0
30
60
90
120
150
180
φ(degrees)

Figure 1:

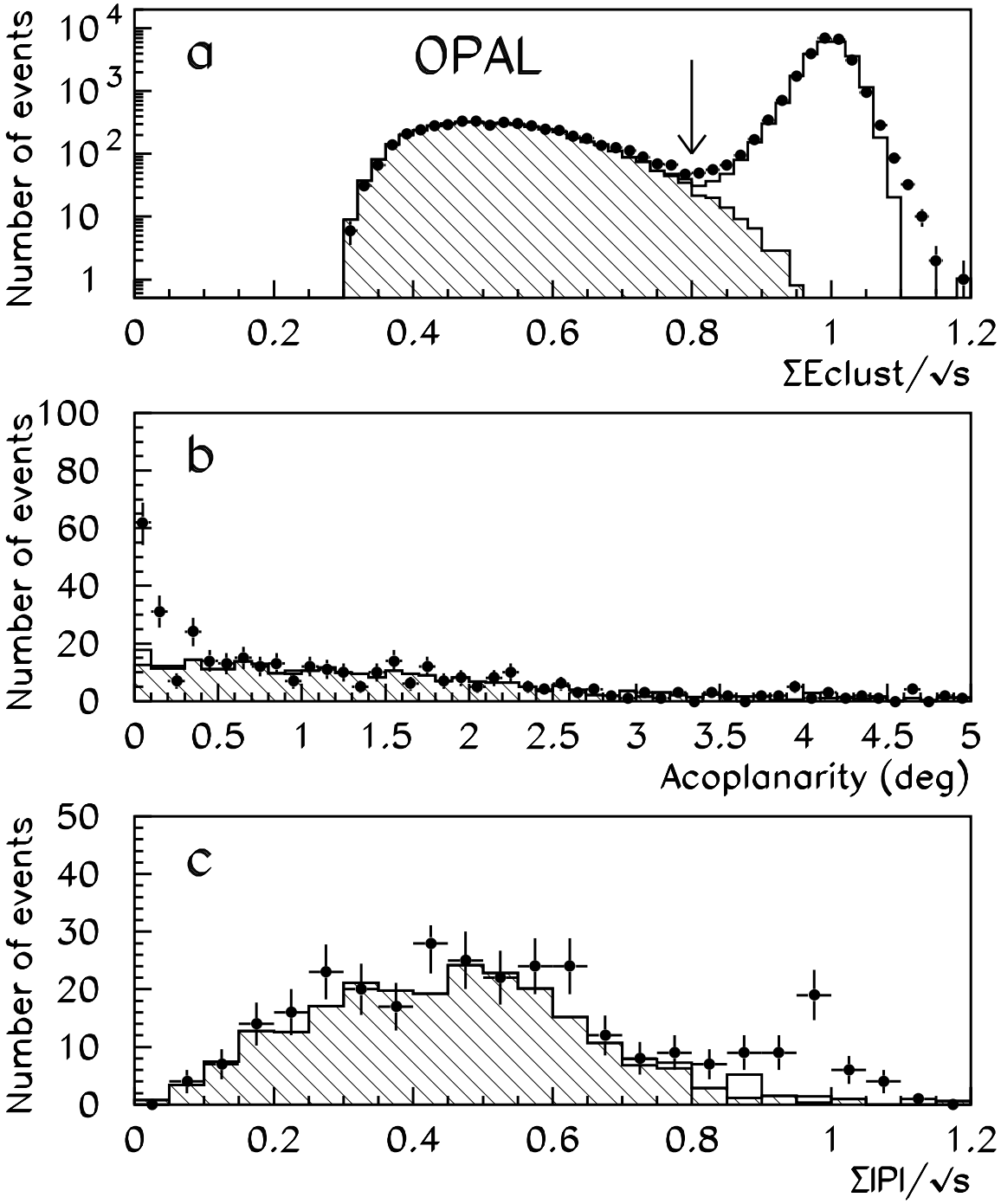
a
OPAL
Number of events
ΣEclust/√s
b
Number of events
Acoplanarity (deg)
c
Number of events
Σ|P|/√s

Figure 2:

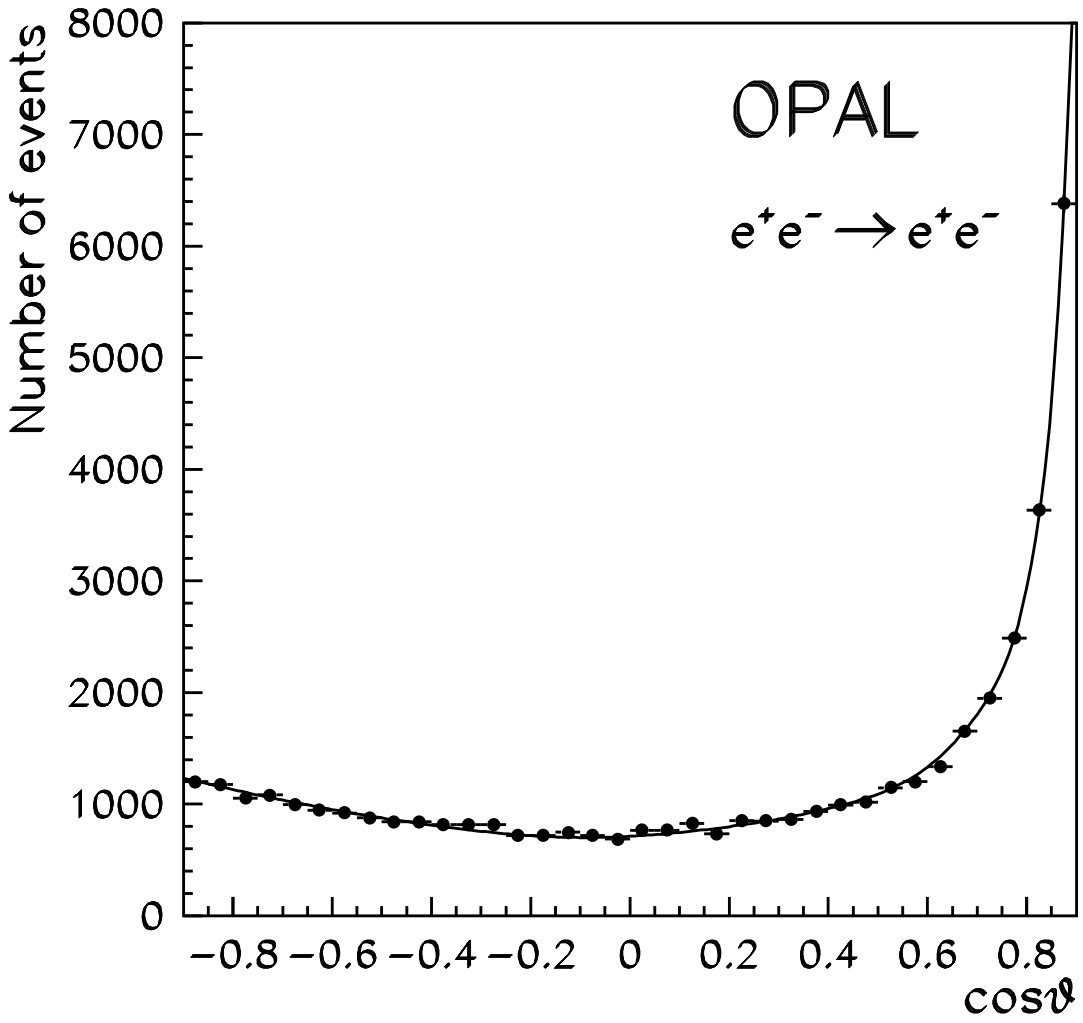
OPAL
$e^+e^- \rightarrow e^+e^-$
Number of events
8000
7000
6000
5000
4000
3000
2000
1000
0
−0.8 −0.6 −0.4 −0.2 0 0.2 0.4 0.6 0.8
cosϑ

Figure 3:

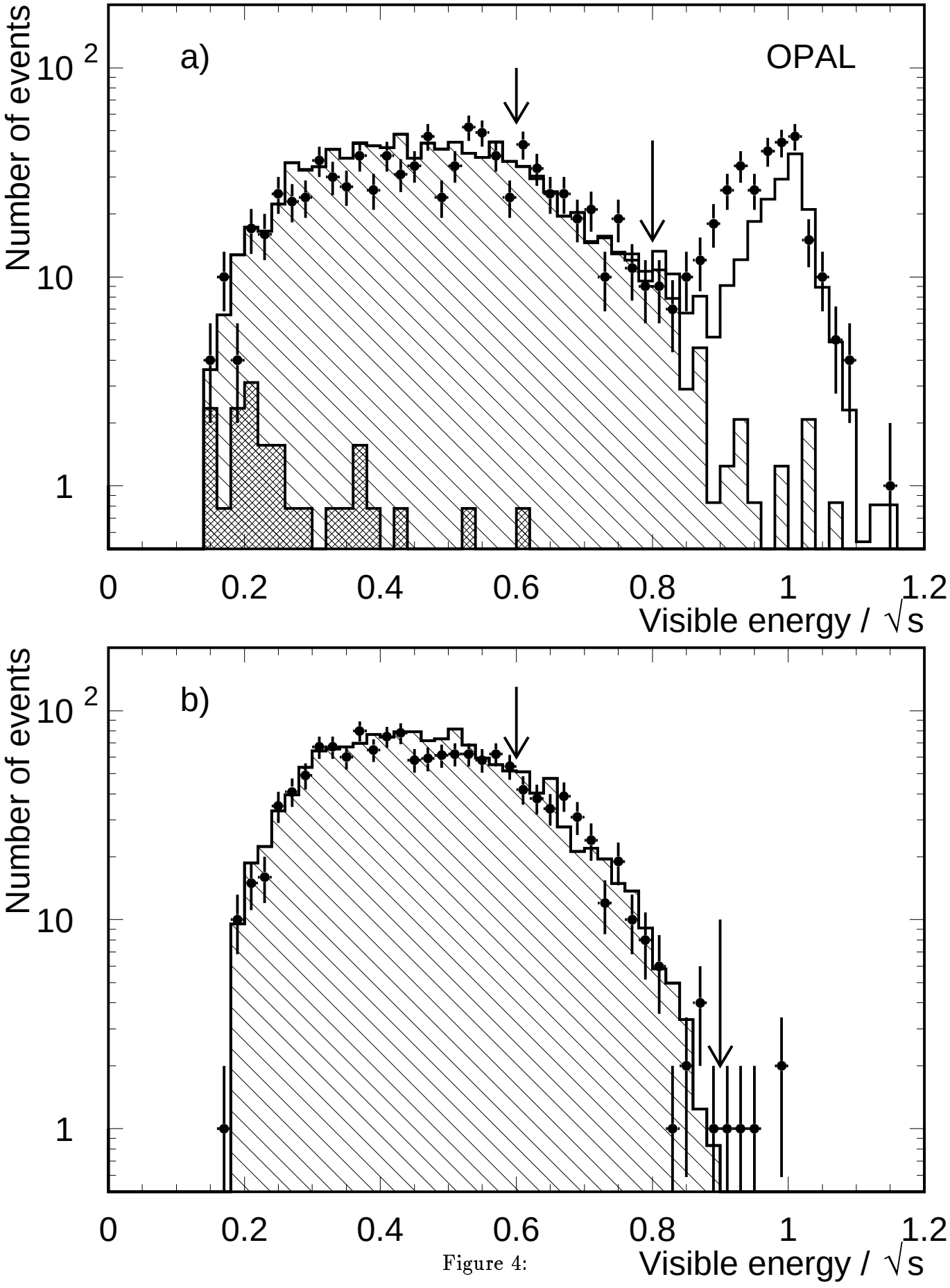
a)
OPAL
Number of events
10^2
10
1
0
0.2
0.4
0.6
0.8
1
1.2
Visible energy / $\sqrt{s}$
b)
Number of events
10^2
10
1
0
0.2
0.4
0.6
0.8
1
1.2
Visible energy / $\sqrt{s}$

Figure 4:

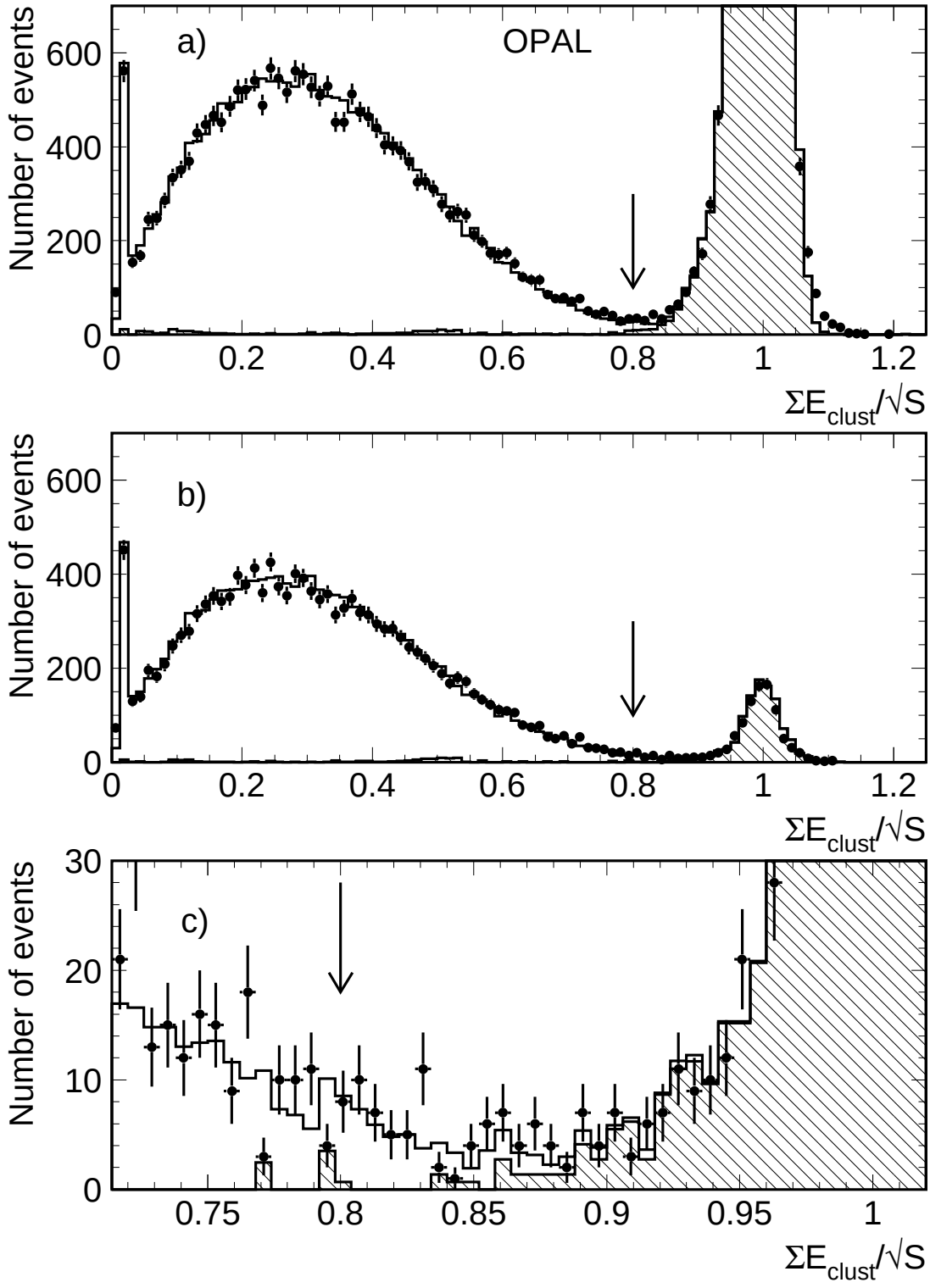
a)
OPAL
Number of events
600
400
200
0
0
0.2
0.4
0.6
0.8
1
1.2
ΣE_clust/√S
b)
Number of events
600
400
200
0
0
0.2
0.4
0.6
0.8
1
1.2
ΣE_clust/√S
c)
Number of events
30
20
10
0
0.75
0.8
0.85
0.9
0.95
1
ΣE_clust/√S

Figure 5:

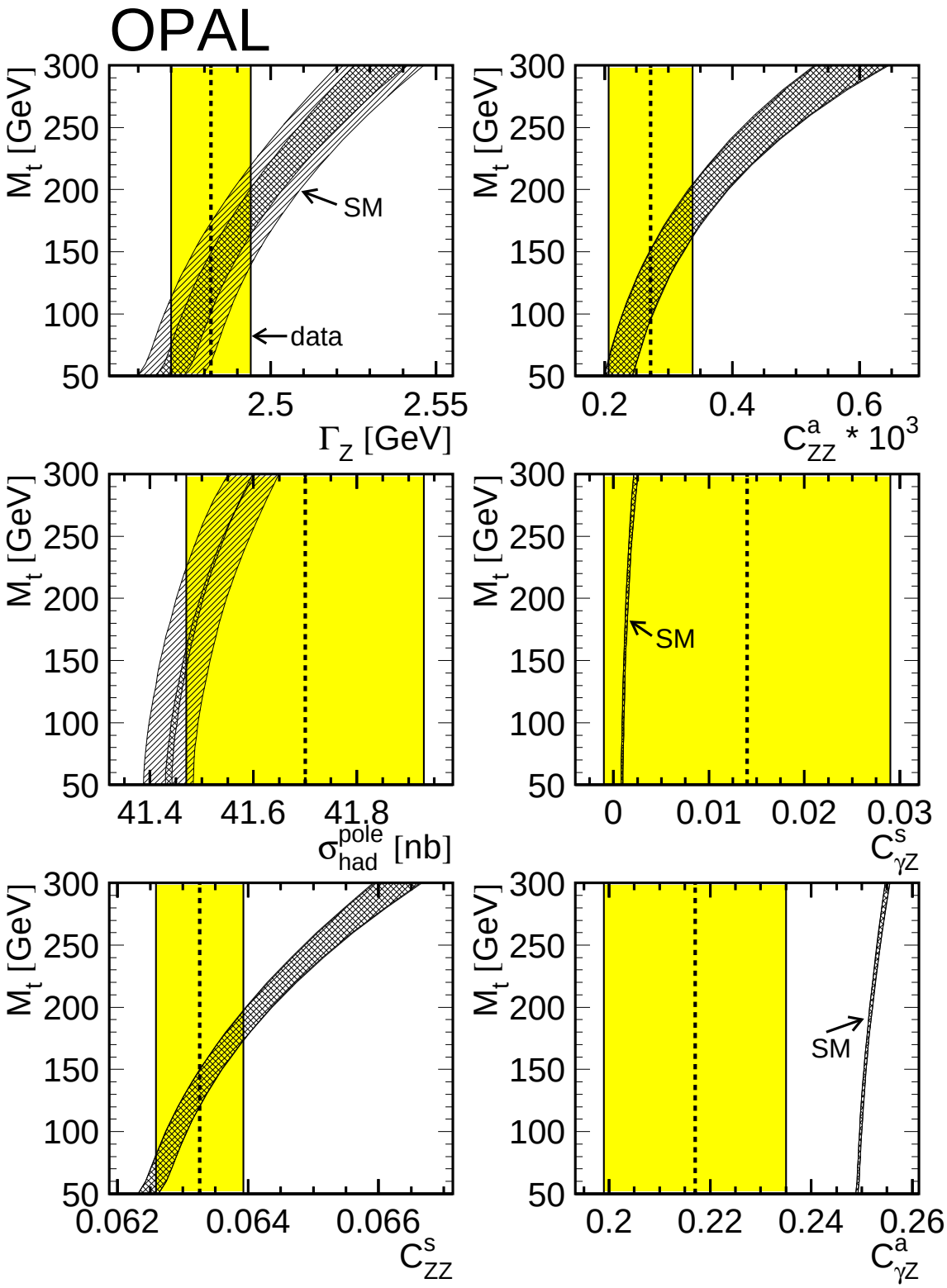
OPAL
M_t [GeV]
300
250
200
150
100
50
SM
data
2.5
2.55
Γ_Z [GeV]
0.2
0.4
0.6
$C^a_{ZZ} * 10^3$
41.4
41.6
41.8
σ^{pole}_{had} [nb]
0
0.01
0.02
0.03
$C^s_{\gamma Z}$
0.062
0.064
0.066
C^s_{ZZ}
0.2
0.22
0.24
0.26
$C^a_{\gamma Z}$

Figure 6:

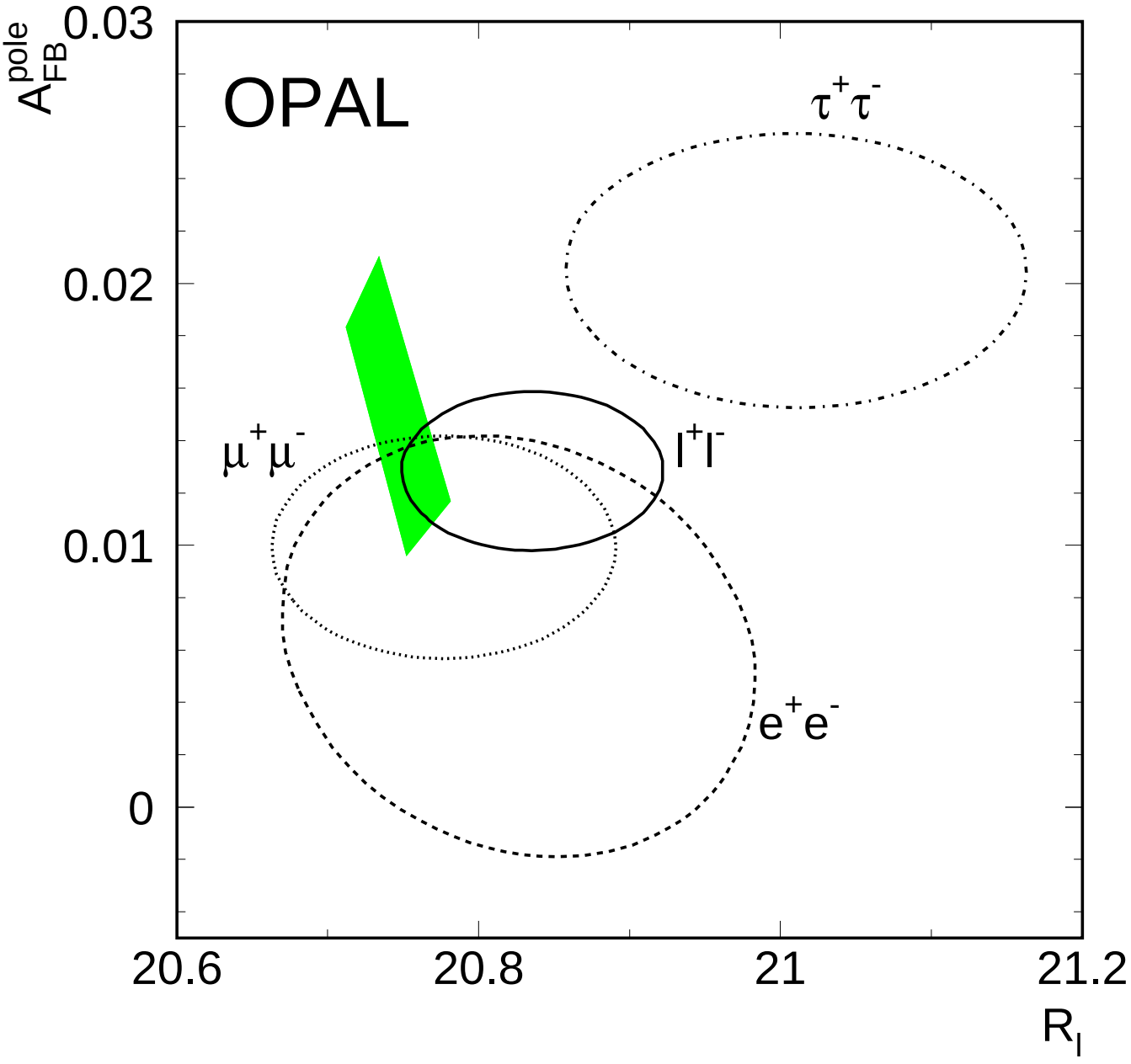

Figure 7:

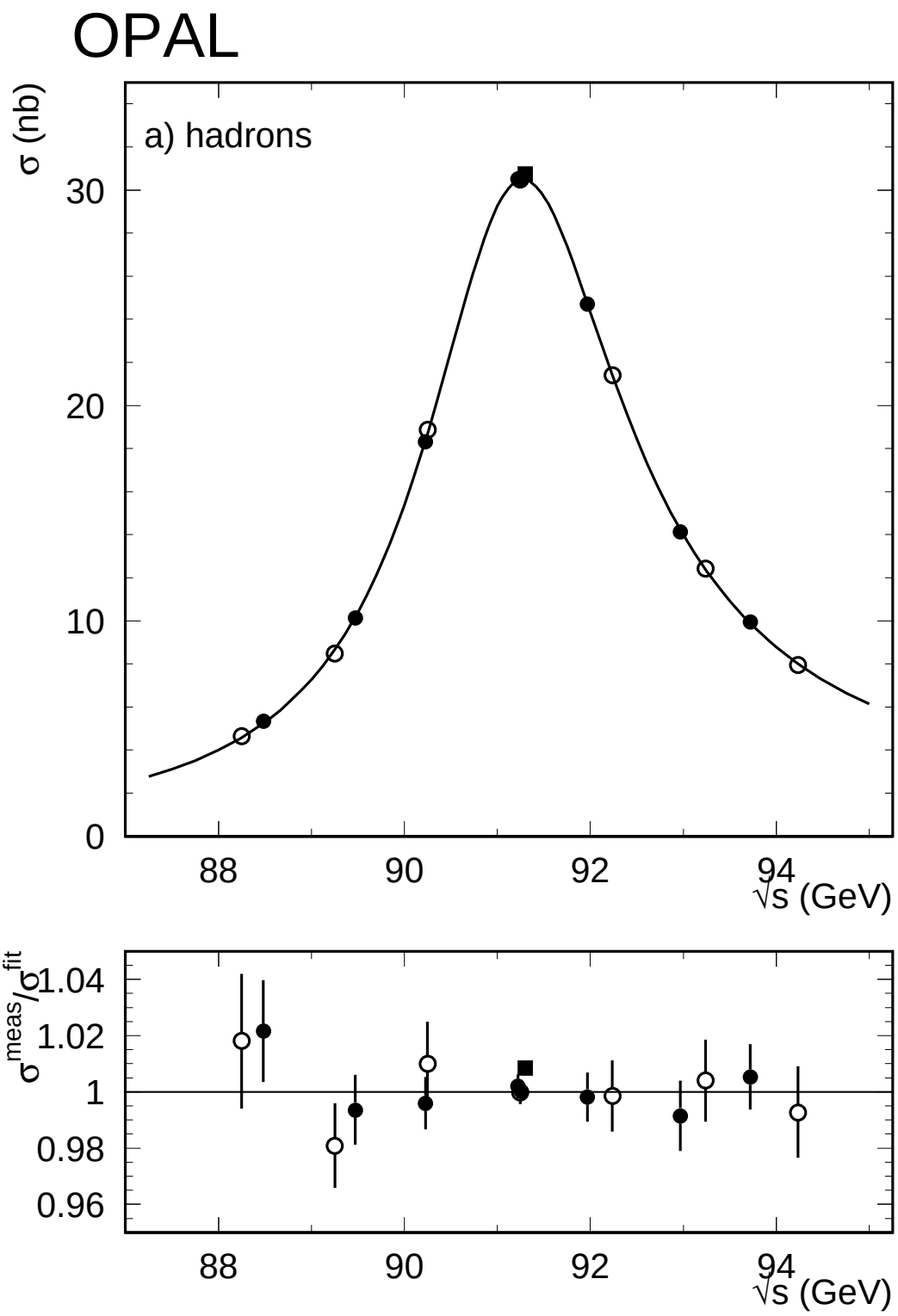
OPAL
a) hadrons
σ (nb)
30
20
10
0
88
90
92
94
√s (GeV)
σ^meas/σ^fit
1.04
1.02
1
0.98
0.96
88
90
92
94
√s (GeV)

Figure 8:

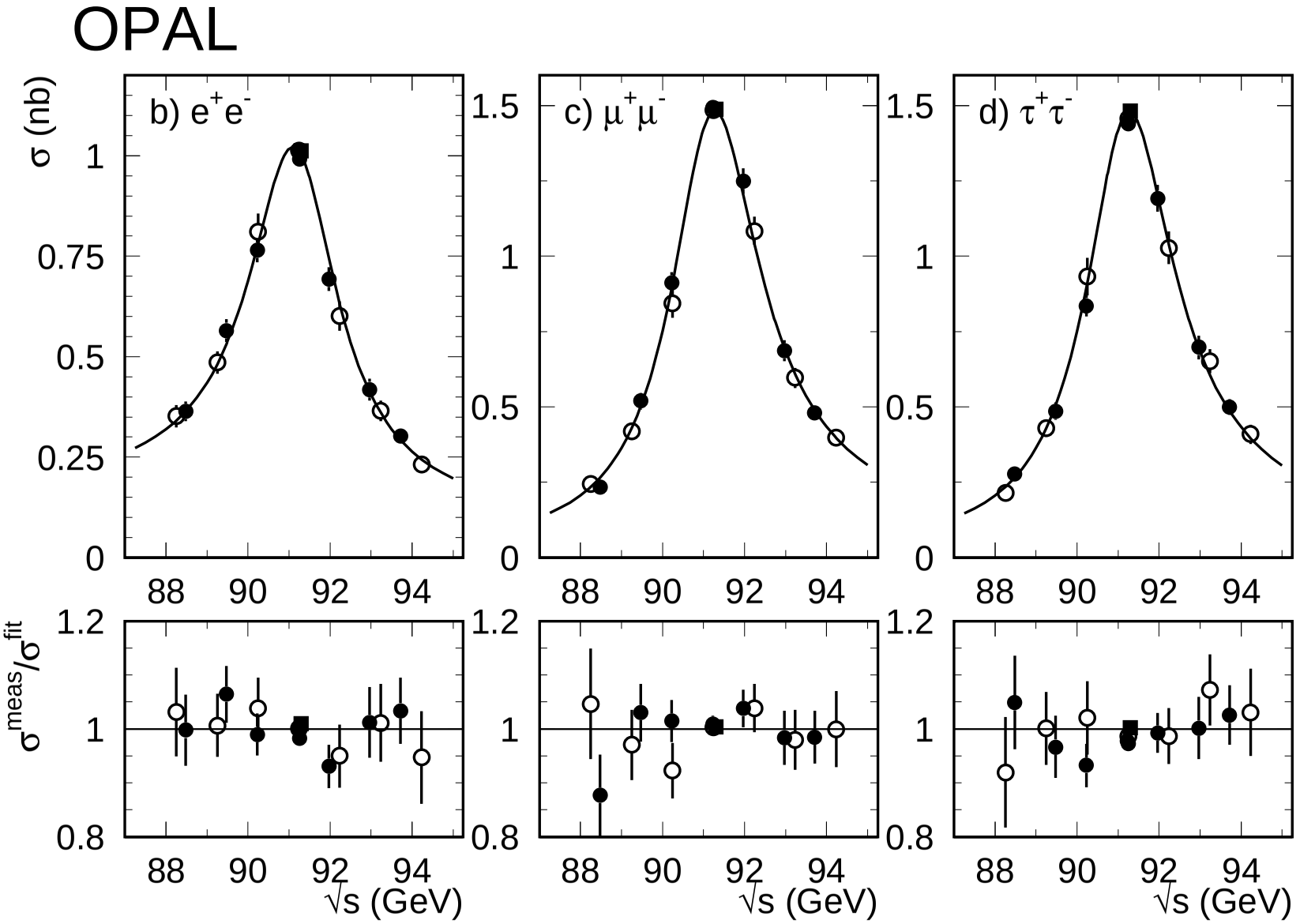

Figure 8:

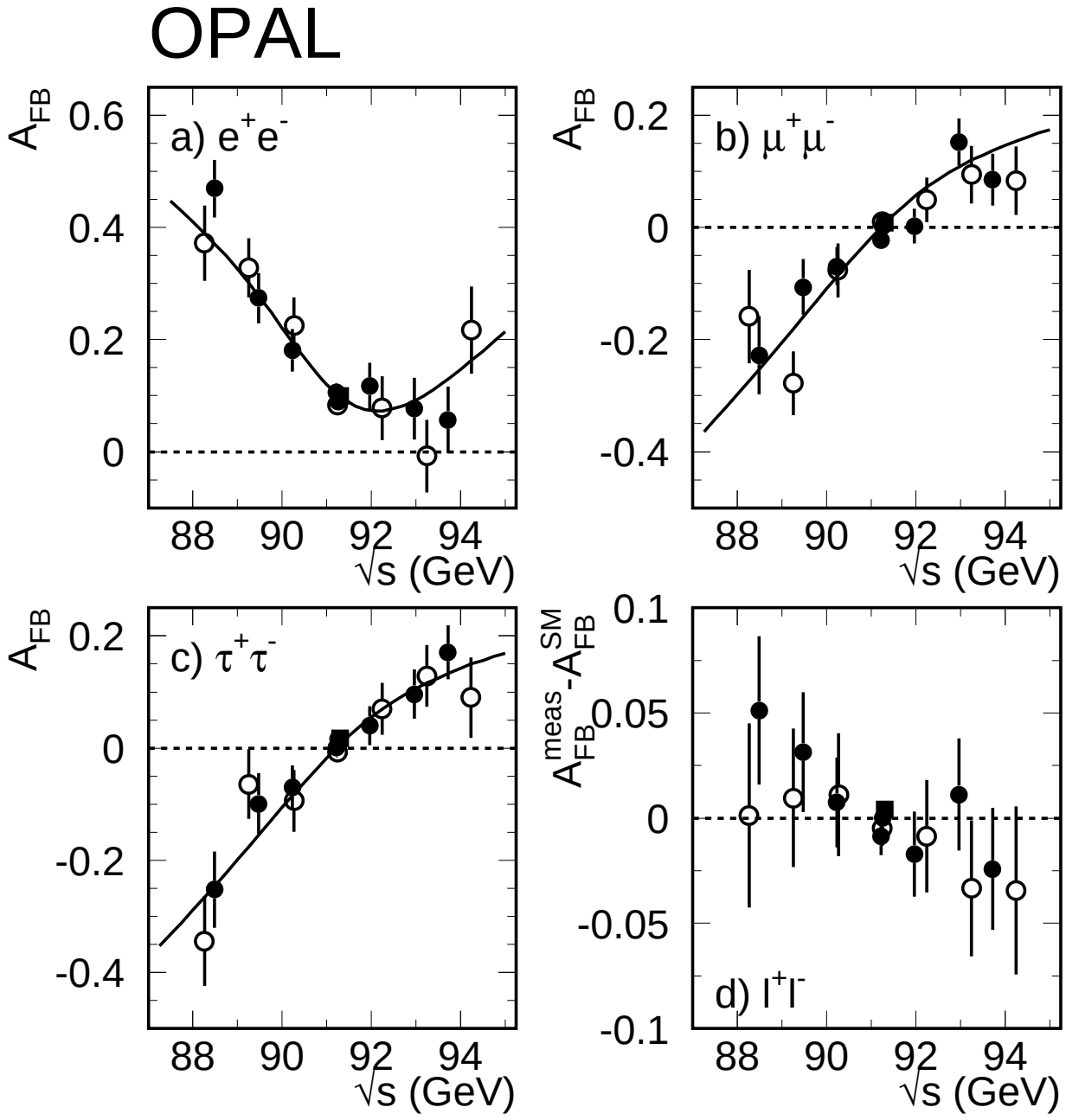
OPAL
A_{FB}
a) e^+e^-
b) $\mu^+\mu^-$
c) $\tau^+\tau^-$
d) l^+l^-
A_{FB}^{meas}-A_{FB}^{SM}
√s (GeV)
88
90
92
94
0.6
0.4
0.2
0
-0.2
-0.4
0.1
0.05
-0.05
-0.1

Figure 9:

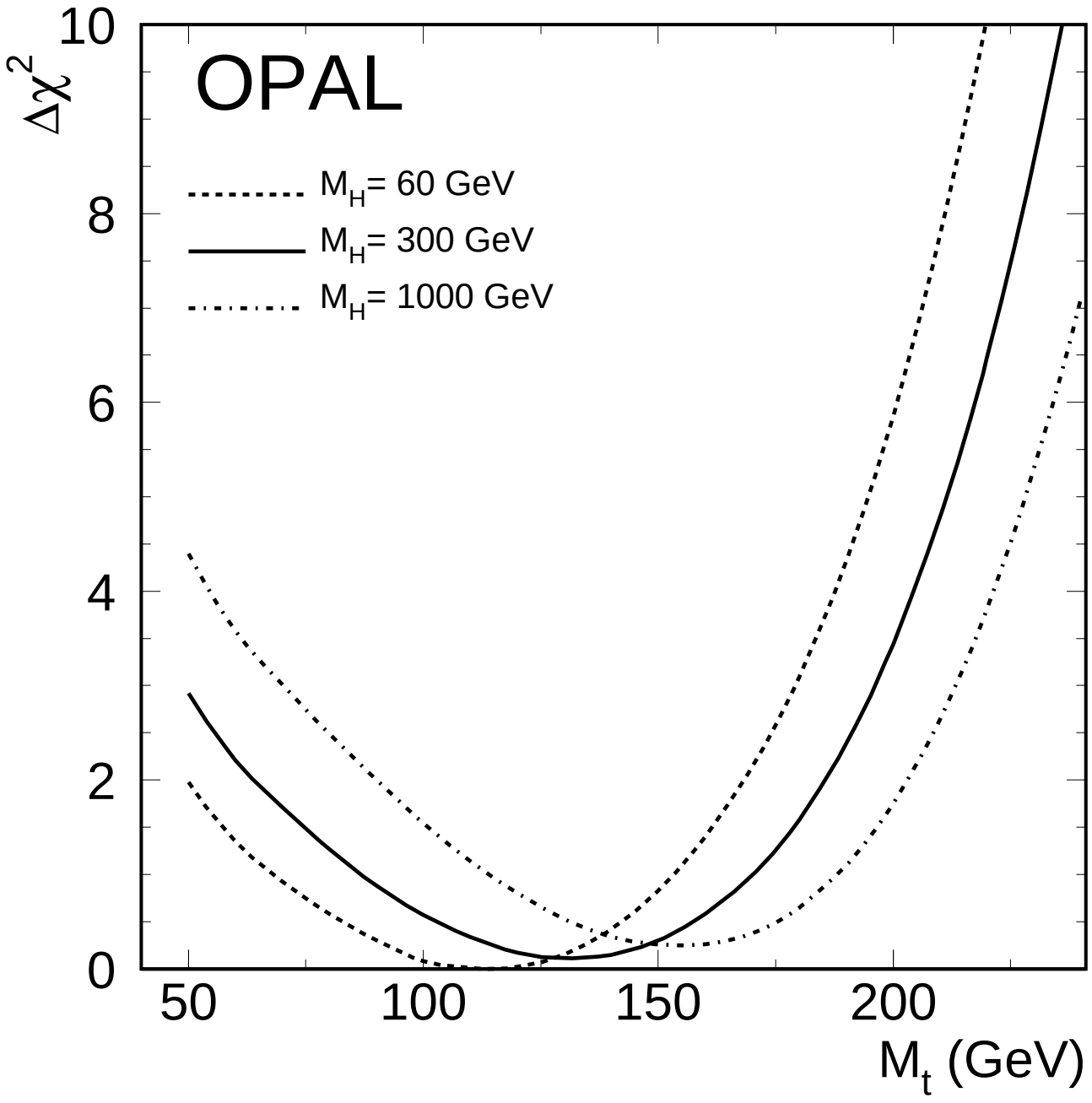
OPAL
$\Delta\chi^2$
M_H= 60 GeV
M_H= 300 GeV
M_H= 1000 GeV
M_t (GeV)
0
2
4
6
8
10
50
100
150
200

Figure 10:

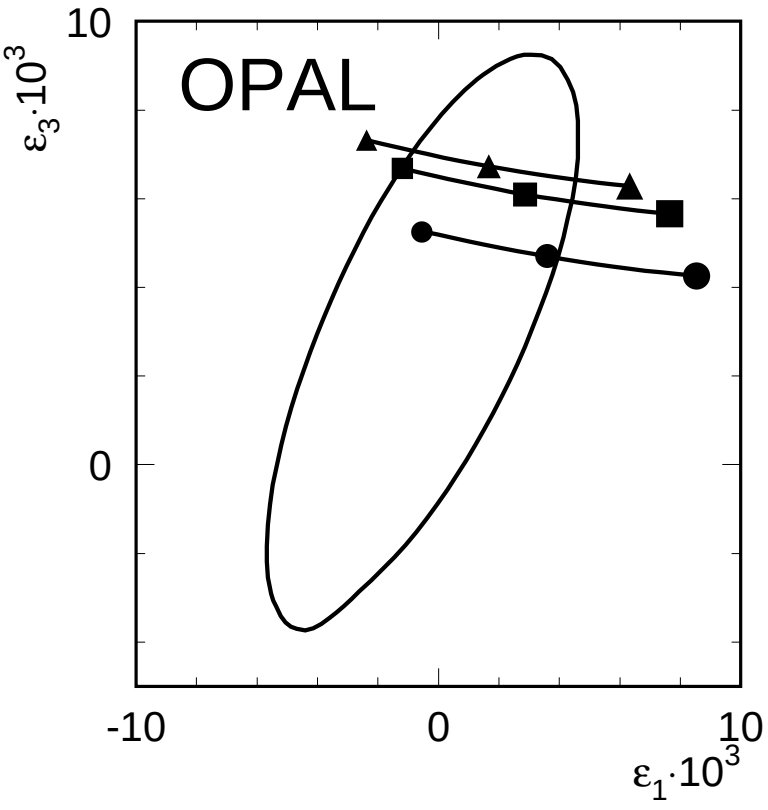

Figure 11: